land

MDPI

Article

Synergistic Use of Synthetic Aperture Radar Interferometry and Geomorphological Analysis in Slow-Moving Landslide Investigation in the Northern Apennines (Italy)

Carlotta Parenti [1,2], Francesca Grassi [2,3,*], Paolo Rossi [2,3], Mauro Soldati [1,2], Edda Pattuzzi [4] and Francesco Mancini [2,3]

[1] Department of Chemical and Geological Sciences, University of Modena and Reggio Emilia, Via Campi 103, 41125 Modena, Italy; carlotta.parenti@unimore.it (C.P.); mauro.soldati@unimore.it (M.S.)
[2] CRICT—Inter-Departmental Research and Innovation Centre on Constructions and Environmental Services, University of Modena and Reggio Emilia, Via Vivarelli 10, 41125 Modena, Italy; paolo.rossi@unimore.it (P.R.); francesco.mancini@unimore.it (F.M.)
[3] Department of Engineering "Enzo Ferrari", University of Modena and Reggio Emilia, Via Vivarelli 10, 41125 Modena, Italy
[4] Regional Agency for Territorial Safety and Civil Protection of Emilia-Romagna, Viale Silvani 6, 40122 Bologna, Italy; edda.pattuzzi@regione.emilia-romagna.it
* Correspondence: francesca.grassi94@unimore.it; Tel.: +39-059-205-6334

Abstract: In mountain environments, landslide activity can be assessed through a combination of remote and proximal sensing techniques performed at different scales. The complementarity of methods and the synergistic use of data can be crucial for landslide recognition and monitoring. This paper explored the potential of Multi-Temporal Differential Synthetic Aperture Radar Interferometry (MT-DInSAR) to detect and monitor slope deformations at the basin scale in a catchment area of the Northern Apennines (Italy) and verified the consistency between the landslide classification by the Inventory of Landslide Phenomena in Italy (IFFI) and displacements from the SAR data. In this research, C- and X-band SAR were considered to provide insights into the performances and suitability of sensors operating at different frequencies. This study provides clues about the state of activity of slow-moving landslides and critically assessed its contribution to the IFFI inventory update. Moreover, it demonstrated the benefits of the synergistic use of SAR and geomorphological analysis to investigate slope dynamics in clayey terrains by exemplifying the approach for a relevant case study, the Gaiato landslide. Notwithstanding the widespread use of MT-DInSAR for landslide kinematics investigations, the main limiting factors are discussed along with the expected improvements related to the upcoming new generations of L-band SAR satellites.

Keywords: SAR interferometry; slope dynamics; landslide recognition; Northern Apennines, Italy

Citation: Parenti, C.; Grassi, F.; Rossi, P.; Soldati, M.; Pattuzzi, E.; Mancini, F. Synergistic Use of Synthetic Aperture Radar Interferometry and Geomorphological Analysis in Slow-Moving Landslide Investigation in the Northern Apennines (Italy). *Land* **2024**, *13*, 1505. https://doi.org/10.3390/land13091505

Academic Editor: Deodato Tapete

Received: 31 July 2024
Revised: 7 September 2024
Accepted: 13 September 2024
Published: 16 September 2024

1. Introduction

In mountainous areas, landslides cause significant landscape changes and can be the main geological hazard generating fatalities, damage to infrastructures, and high economic losses. Landslide occurrence can be favored by different predisposing factors (e.g., lithology, topography, and faults), and triggered by different processes, such as soil erosion, tectonic activity, intense rainfall, or anthropogenic activities like excavations, agriculture, and mining [1–3].

This paper focuses on slow-moving landslides [4,5]. Slow-moving landslides are usually found in hilly–mountainous areas characterized by mechanically weak lithologies [6–8]. They exhibit gradual movement through time, with velocities ranging from mm year^{-1} to m year^{-1} for months to hundreds of years [1,8].

The investigation and assessment of slow-moving landslides requires a multi-scale and multidisciplinary methodological approach and usually includes landslide inventories [9–12],

multitemporal monitoring [13–17], and long-term and short-term analysis aiming to define and characterize the state of activity and evolution of the slope movements [18–23]. Several methodologies can be implemented for the monitoring of landslide properties and evolution, such as ground-based topography and geodesy, geotechnical investigations, aerial proximal sensing, and Earth Observation (EO)-based techniques [24], together with a variety of in situ approaches and their integrated uses [21,25–28]. Among these, technologies based on Global Navigation Satellite Systems (GNSS), terrestrial laser scanning, total stations, geotechnical sensors (e.g., inclinometers, piezometers, extensometers etc.) and Uncrewed Aerial Vehicles (UAVs) photogrammetry and LiDAR are commonly implemented. In particular, UAV-based surveys are very effective for monitoring natural processes as they allow for the generation of high-resolution 3D models at repeated intervals (months or years) for morphological applications and investigation of slope dynamics. On the contrary, point-based methodologies, such as GNSS and a total station, can be adopted for in situ monitoring and whenever the establishment of a reference frame is required [29].

Satellite radar interferometric techniques have been widely used in EO applications for their ability to provide the surface displacement components oriented along the Line of Sight (LOS) direction to a large extent with centimeter to millimeter accuracy [30]. The first applications of the Differential Synthetic Aperture Radar Interferometry (DInSAR) included the mapping of displacement fields caused by earthquakes, volcanic activities, ice sheet flow [31], and landslide detection and monitoring [32]. The combination of a long series of radar satellite data and of advanced multi-temporal techniques [33–36] now permits the investigation of the evolution of these phenomena. The displacement of selected targets, the so-called Persistent Scatterers (PS), can be determined with an accuracy on the order of 1–2 mm/year for velocities extrapolated from time series [37].

For the abovementioned reasons, the ability of SAR interferometry to detect slow-moving landslides has been widely exploited [38–43]. In addition, the technique is able to retrieve displacements from data acquired by constellations of satellites operating at multi-frequencies (namely the L, C, and X frequency bands) and varying spatial resolutions.

For the purposes of the proposed research, the Sentinel-1 (S1) C-band constellation (European Space Agency, ESA) and the X-band COnstellation of small Satellites for Mediterranean basin Observation (COSMO-SkyMed) (Italian Space Agency, ASI) need to be mentioned. It is important to highlight the advantages and drawbacks related to the use of the different systems operating at different frequencies. Radar data acquired at higher frequencies (i.e., X-band and, secondly, C-band) ensure lower phase noise as their value decreases with the signal wavelength; on the other hand, data acquired at lower frequencies (i.e., L-band) are less sensitive to temporal decorrelation as longer wavelengths ensure higher coherence values between image pairs and exhibit an increased capability to penetrate the vegetation canopy. Moreover, the maximum detectable displacement between two successive passes along the line of sight is strongly related to the signal wavelength as its value is equal to $\lambda/4$ (where λ is the signal wavelength) [30,44]. Thus, when dealing with landslide monitoring in a vegetated environment, the use of SAR data from a satellite operating at a longer wavelength is advised [45,46]. This is especially pertinent for faster slope deformation processes, as evidenced, for instance, by Strozzi et al., 2005 [25], who demonstrated the capabilities of L-band JERS data over the Italian and Swiss Alps. Other limitations can be attributed to geometrical and morpho-structural settings, slope orientation, and exposure with respect to the satellite acquisition geometry, including the occurrence of shadowing [28].

The aim of the present research was to verify the efficiency and potentialities of multi-frequency and dual-geometry SAR interferometry to detect and monitor slope deformations at a basin scale in a catchment area of the Northern Apennines (Italy) and assess the state of activity of landslides by monitoring their evolution through time. This is pursued through the exploitation of dual-orbit datasets from C-band S1 and X-band CSK Constellations. The investigated area is the Scoltenna Stream catchment in the Modena Apennines (Emilia-Romagna, Italy). This area is characterized by a high incidence of landslides, which vary

in type and size, and a significant propensity for slope instability [47]. The ability of SAR interferometry to detect surface deformations in areas with locally dominant land covers and the assessment of results in comparison with the classification of landslides provided by the available landslide inventories will be discussed. Furthermore, an in-depth and exhaustive analysis of a relevant landslide located in the study area, the Gaiato landslide, is presented to more clearly delineate the aforementioned potentialities of SAR interferometry in a multidisciplinary approach.

2. Study Area

The Scoltenna Stream catchment is located in the Northern Apennines (Modena Province, Italy) and has an extent of about 280 km^2 and an elevation ranging from 300 to 2000 m above sea level (a.s.l.) (Figure 1). The Scoltenna Stream originates near Pievepelago from the confluence of the Perticara, Tagliole and Pozze streams. The Scoltenna Stream is 33 km long, with an average flow rate of 3.5 m^3/s and an active channel width ranging between 10 m and 85 m [29]. The hydrographic network is strongly controlled by the physiographic conditions of the valley, with a prevalence of sinuous pattern.

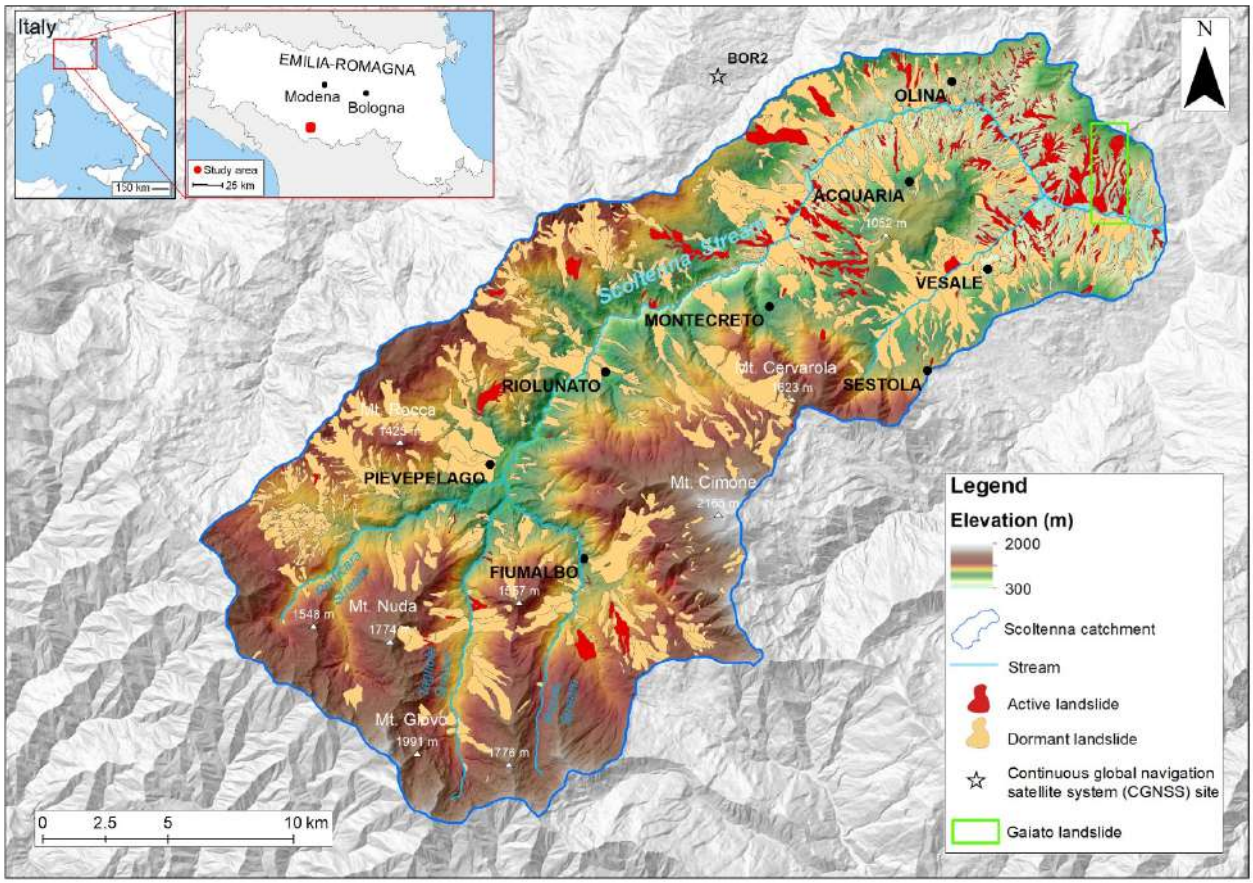

Figure 1. Location and physiographic aspects of the Scoltenna Stream catchment (Modena Apennines, Italy) and landslides of the IFFI inventory (available online: https://geoportale.regione.emilia-romagna.it/ accessed 10 May 2024).

2.1. Geological and Geomorphological Setting

Geologically, the Modena Apennines belong to a fold-and-thrust mountain range derived from the complex and multi-staged evolution of the post-Eocene collision between the European and African plates [48,49]. The southern part of the Scoltenna Stream catchment is characterized by calcareous–marly formations, while the northern part is composed by arenaceous–clayey formations (flysch) [21].

The geological units outcropping in the catchment show a remarkable predisposition to slope instability. Erosion processes influence and decrease the mechanical properties of the geological formations and facilitate progressive water absorption, making the slopes prone to landslide processes [50,51]. The main predisposing factors for landslide occurrence can be related to the prevalent clayey nature of the rocks and to intense and/or prolonged rainfall concentrated in the autumn and spring periods. The types of landslides are determined by the geological–structural properties of the formations involved. Landslides are generally composed of thick clayey deposits with gravel and blocks due to the weathering of claystone, sandstone, and limestone rocks. Landslides can evolve through multiple and/or successive movements with partial and/or total reactivations. The reactivations can be due to (a) failures at the crown zone, (b) undrained loading of pre-existing landslide deposits, and (c) downslope failure propagation of the entire landslide body [52,53]. All landslide types can be recognized in the study area, but the most frequent are slow-moving earth slides and earth flows [21,54–59]. In the Scoltenna catchment, 1239 landslides were identified, 393 are active (31.7%) and the remaining 846 are dormant (68.3%) [60].

2.2. Climatic Setting

According to the Köppen classification [61] the climate of the Scoltenna catchment is defined as "sub-continental" and locally as "cool-temperate" with a mild temperate climate (Cfa). The area presents a Mediterranean climate and is characterized by intense rainfall in spring and autumn and dry summers and winters with moderate precipitation and/or snowfall [62–64]. Rainfall is generally one of the main factors triggering the reactivation of landslides, especially during autumn and spring when intense precipitation can last for several days, which is becoming more common due to recent climate changes [53,65].

2.3. The Gaiato Landslide Case Study

A relevant case study, the Gaiato landslide, was deeply investigated to better assess the potentialities of SAR interferometry and a multidisciplinary approach. The Gaiato landslide (Figure 1) is located in the lower Scoltenna catchment and is characterized by clay terrains. It is classified as earth flow, but detachment from the sub-vertically fractured calcarenites can lead to rock falls and block slides. The infiltration of rainfall in the fracture networks can lead to the reactivation of a deep ruptured surface, eventually reaching the less permeable clay formations underneath that become more plastic [66,67]. An important role is also played by the runoff waters, which cause rapid incision of the slope due to the high erodibility of the soil with consequent degradation and erosion of the surface and slope processes. The current conditions of the Gaiato landslide does not represent a hazardous situation due to the absence of settlements in the immediate vicinity but a foreseeable progressive regression of the crown of the landslide, due to subsequent collapses, could damage the buildings closest to the landslide (including the Tower of Gaiato from the XII century). The most recent movements occurred after intense rainfall between March and April 2013 (available online: https://geoportale.regione.emilia-romagna.it/, accessed on 17 July 2024 [60]).

3. Materials and Methods

This research took advantage of a multidisciplinary approach for the detection, investigation and assessment of slope movements. Cartographic material and different datasets were analyzed: slope instability maps and landslide inventories and catalogs were complemented by satellite radar datasets, and detailed geomorphological surveys were carried out for ground truthing. The flowchart summarizing the proposed approach is presented in Figure 2.

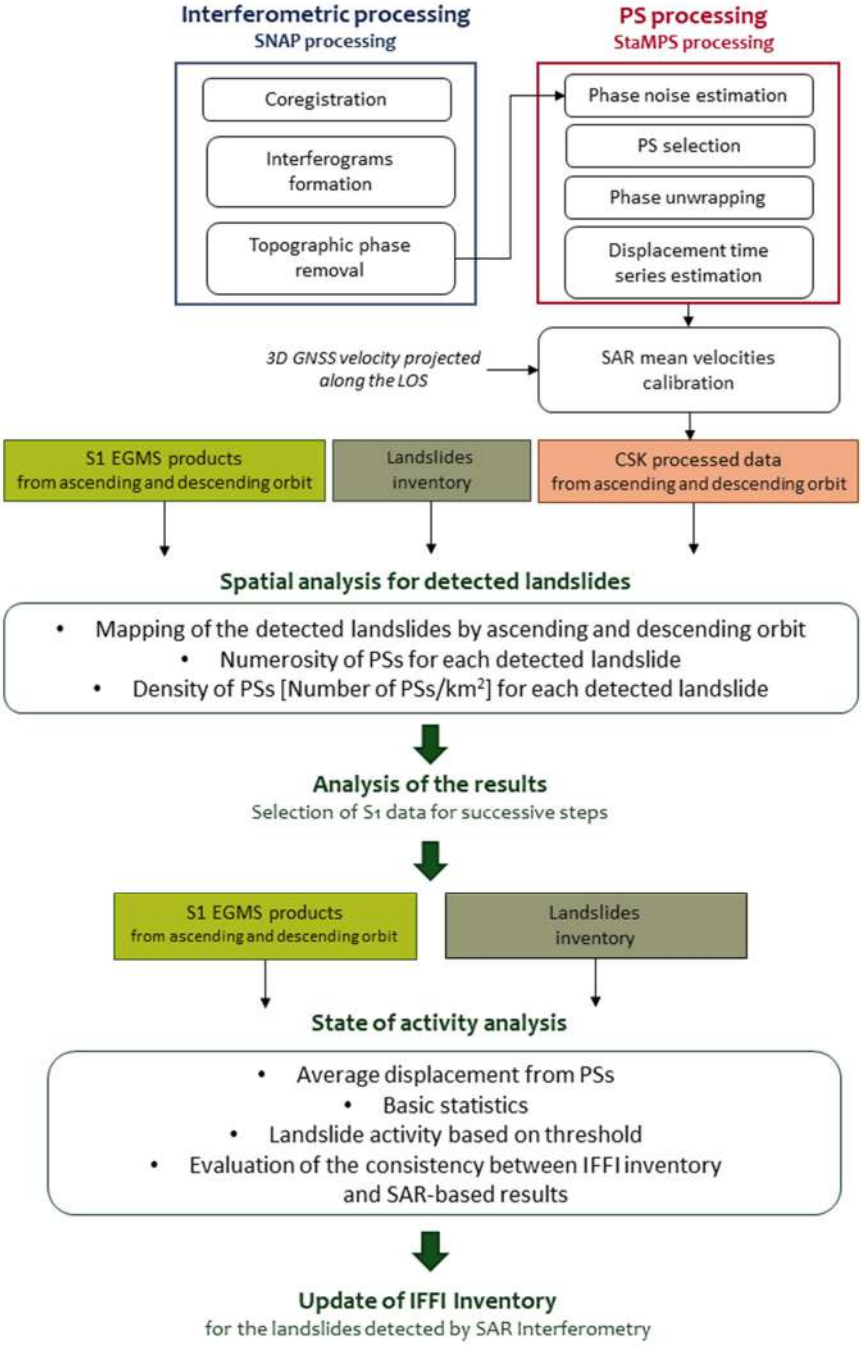

Figure 2. Flowchart describing the SAR processing and the spatial and statistical analysis of multi-temporal interferometric data.

3.1. Cartographic Material

The open-access availability of geospatial datasets and cartographic products, as well as inventories, catalogs, archives, online platforms and digital databases, is rapidly increasing and becoming a useful tool to investigate and assess slope dynamics. Regional, national, or international repositories (e.g., the Italian Regional and National Geoportals) provide different thematic maps, including geological maps and slope instability maps, and landslide inventory maps, historical digital orthophotos, and interferometric data [29]. In this study, the authors collected digital color orthophotos and optical satellite imagery, together with a Digital Elevation Model (DEM) at 5 × 5 m spatial resolution [60] and the Inventory of Landslide Phenomena in Italy (IFFI). The IFFI project by ISPRA (Italian Institute for Environmental Protection and Research) supplies a detailed picture of the

distribution of landslides in Italy [68]. This Inventory is the national and official database on landslides [47]. Since 2005, ISPRA has made the data available in online archives to encourage the widest dissemination and utilization of the information by citizens, local administrations, researchers and technicians engaged in the field of territorial and land use planning. Moreover, orthophotos accessible via the Regional Web Map Service were analyzed in a multitemporal perspective in order to investigate and monitor the evolution of the Gaiato landslide. The following years were considered in the analysis: 2008, 2011, 2018 and 2020. The multi-temporal mapping of the landslides was conducted in a GIS environment through a manual delineation method. For each orthophoto in the landslide polygon, the state of activity and land use were mapped. The latter was divided into the following classes: woods, bushes (high and low density), grass, and bare soil.

3.2. Sentinel-1 Constellation and European Ground Motion Service

The major ESA EO program, the Copernicus, includes a constellation of C-band SAR satellites, composed of the Sentinel-1A (S1A) and -1B (S1B) launched in 2014 and 2016, respectively. The data distribution policy of the ESA led to the free availability of a large amount of SAR data worldwide at average spatial resolution and very short revisit times. In the Interferometric Wide (IW) acquisition mode, a resolution of 5 m $\times$ 20 m was achieved and a 6 day revisit time is available when the ensembled S1 constellation is considered [69]. In addition to the open datasets, ESA released a trusted tool for the processing of data provided by the Sentinels constellation, the Sentinel Application Platform (SNAP) software (version 9.0.0 was used in this work), which includes interferometric utilities, complemented by the Statistical Cost Network Flow Algorithm for Phase Unwrapping (SNAPHU) package for phase unwrapping [70].

In addition, the open-source distribution strategy of the S1 data paved the way for the development of a ground deformation service for the monitoring of the entire European territory, the European Ground Motion Service (EGMS) [71,72]. The objective of the EGMS is to provide standardized, consistent, interoperable and harmonized ground motion data combining the most advanced Multi-Temporal DInSAR (MT-DInSAR) processing techniques of dual-orbit S1 data available from the beginning of the mission (i.e., 2015) and high-quality GNSS models to calibrate the products [73]. The EGMS provides deformation maps and displacement time series of single targets updated on a yearly basis. The main products of the service are: (a) the GNSS-calibrated deformation maps and time series along the radar LOS and (b) the decomposed (east–west oriented and vertical) deformation maps at a spatial resolution of 100 m $\times$ 100 m.

To achieve the objectives of this research work, the calibrated LOS-oriented products have been considered to preserve the full resolution of the S1 data and to provide measurements relative to an absolute reference frame. In particular, products from both ascending (117 passes) and descending (168 passes) orbits related to the period 2015–2021 were downloaded from the EGMS Explorer and imported in a GIS project [74].

3.3. COSMO-SkyMed Constellations and Data Processing over the Scoltenna Catchment

The COSMO-SkyMed (CSK) is the ASI main EO system, whose aim is to provide data and products for scientific, defense and commercial applications and risk management [75]. The CSK first generation mission reached full operational capabilities in 2011 and is composed of a constellation of four satellites equipped with a multi-mode high resolution X-band SAR. The first generation constellation is currently being complemented by the COSMO-SkyMed Second Generation (CSG), a constellation of two enhanced SAR satellites conceived to ensure the operational continuity to the CSK and to improve the data in terms of spatial resolution, number of available images and available sensing modes [76]. For this research, a dual orbit CSK dataset was requested from ASI through the new portal for Italian Institutional Users. This portal allows registered users to obtain free access to CSK and CSG data after submitting a project proposal [77]. An ascending dataset (spanning the years 2012–2022) and a descending one (from 2012 to 2021) was

requested for the Scoltenna catchment. The dataset is composed of Single-look Complex Slant (SCS) weighted and radiometrically equalized (Level 1A) data acquired with the Stripmap Himage mode. The data have a spatial resolution of 3 m in both range and azimuth directions. Further information regarding the CSK dataset can be found in Table 1.

Table 1. Information regarding the CSK dataset over the Scoltenna catchment.

Orbit Type	Number of Products	Acquisition Time	Scene Center [Lat, Lon]	Start Date	End Date	Master Date	Mean Temporal Baseline
Ascending	92	04:46 UTC	[44.2581487, 10.65246370]	03/03/2012	22/08/2022	01/03/2017	41 days
Descending	50	17:20 UTC	[44.25349403, 10.70065910]	07/05/2012	05/12/2021	07/10/2015	70 days

The ascending and descending orbits were then processed using an open-source procedure that combines SNAP, the Stanford Method for Persistent Scatterers (StaMPS) [78], and the MATLAB routines [79]. The processing strategy aims to compute the displacement history of selected stable targets from a large set of SAR data, achieving a high level of accuracy (1–2 mm/year) using the PS theory presented in Hooper et al., 2004 [35]. In more detail, the SNAP-StaMPS workflow used in the present study is briefly presented in Figure 2. The interferometric processing performed in SNAP included the selection of the master images, the coregistration of images, the interferograms formation and the removal of the topographic component to the phase. Then, the PS processing performed in StaMPS and complemented by MATLAB routines was performed: the PS candidates were selected using an amplitude dispersion value of 0.50; the phase stability of the candidates was evaluated, estimating the phase noise, and the noisy scatterers were discarded accordingly; the phase was unwrapped and corrected; and, finally, the displacement time series was computed. The last step of the SAR processing included the calibration of both orbits exploiting the 3D velocity field of a GNSS station. In particular, the GNSS velocity field was projected along the ascending and descending slant range directions, then the PSs near the station were aligned to the computed GNSS slant-projected velocity value and the entire dataset was then calibrated. For the CSK dataset, the velocity field of the permanent GNSS station BOR2 located in Lama Mocogno (Modena, Italy) from the service provided by the Nevada Geodetic Laboratory [80] has been employed.

3.4. Geomorphological Assessment and Statistical Analysis of Multi-Temporal SAR Data

In a GIS environment, a visual interpretation of digital orthophotos and optical satellite imagery was performed as they proved their ability to retrieve information related to the extension and state of activity of landslides, together with the integration of thematic maps, DEM, and derived hillshade models [81,82].

The Sentinel-1 EGMS and COSMO-SkyMed products available for the study area were retrieved and imported into a GIS project for successive analysis. In addition, a polygon shapefile containing the active and dormant landslides of the Emilia-Romagna Region was also uploaded and the landslides belonging to the Scoltenna catchment were selected. The landslides' location and state of activity were retrieved from the IFFI inventory. The inventory identifies slow-moving earth slides and earth flows (with velocities ranging from mm/year to cm/year) as the most frequent phenomena occurring in the study area. Subsequently, permanent scatterers processed from the data provided by different satellites and orbits, falling into polygons representing active and dormant landslides, were counted. A spatial and statistical analysis based on the density of PSs was performed. Then, an analysis of the state of activity of each landslide was conducted for S1 data only. In particular, the detected landslides for each orbit were grouped according to the state of activity reported in the IFFI inventory (i.e., active and dormant), and for each landslide, the mean velocity of PSs and its standard deviation were computed to evaluate the state of activity. To avoid the effect of isolated and unstable reflectors, only landslides including

a minimum of 3 PSs and an average velocity higher than 2 mm/year were considered. The cited threshold was selected for two main reasons. Firstly, this work investigates landslides characterized by very small displacements, which are common in the study area; secondly, the accuracy achieved by the multi-temporal interferometric technique, and thus the detectability threshold of the technique, is on the order of 1–2 mm/year; therefore, the detected displacements can be considered as meaningful. The results obtained by the described analysis were compared to the state of activity reported by the IFFI inventory. This procedure allows us to assess the potential of the multi-temporal interferometric technique in the investigations of slow moving landslides and updating of the existing inventories.

4. Results

In the study area, the Sentinel-1 EGMS dataset belonging to the ascending orbit (Figure 3) overlaps with 317 landslides of the IFFI inventory. This value represents the 25.6% of the total number of landslides inside the Scoltenna catchment (1239), corresponding to the 58.2% of the total landslides area in the catchment. The remaining 922 landslides (74.4%) do not match with the PSs obtained by the ascending Sentinel-1 EGMS dataset. Among the mentioned 317 landslides, 12.0% are classified by the IFFI inventory as active (38 of the 317) and the remaining 88.0% as dormant (279). It was noted that 22.1% of the landslides contain fewer than 3 PSs (70 of the 317), 32.8% contain 3 to 10 PSs (104 of the 317), 30.3% contain 11 to 50 PSs (96 of the 317), 8.8% contain 51 to 100 PSs (28 of the 317), 5.4% contain 101 to 500 PSs (17 of the 317), and only 0.6% contain more than 500 PSs (2 of the 317) (Figure 4a).

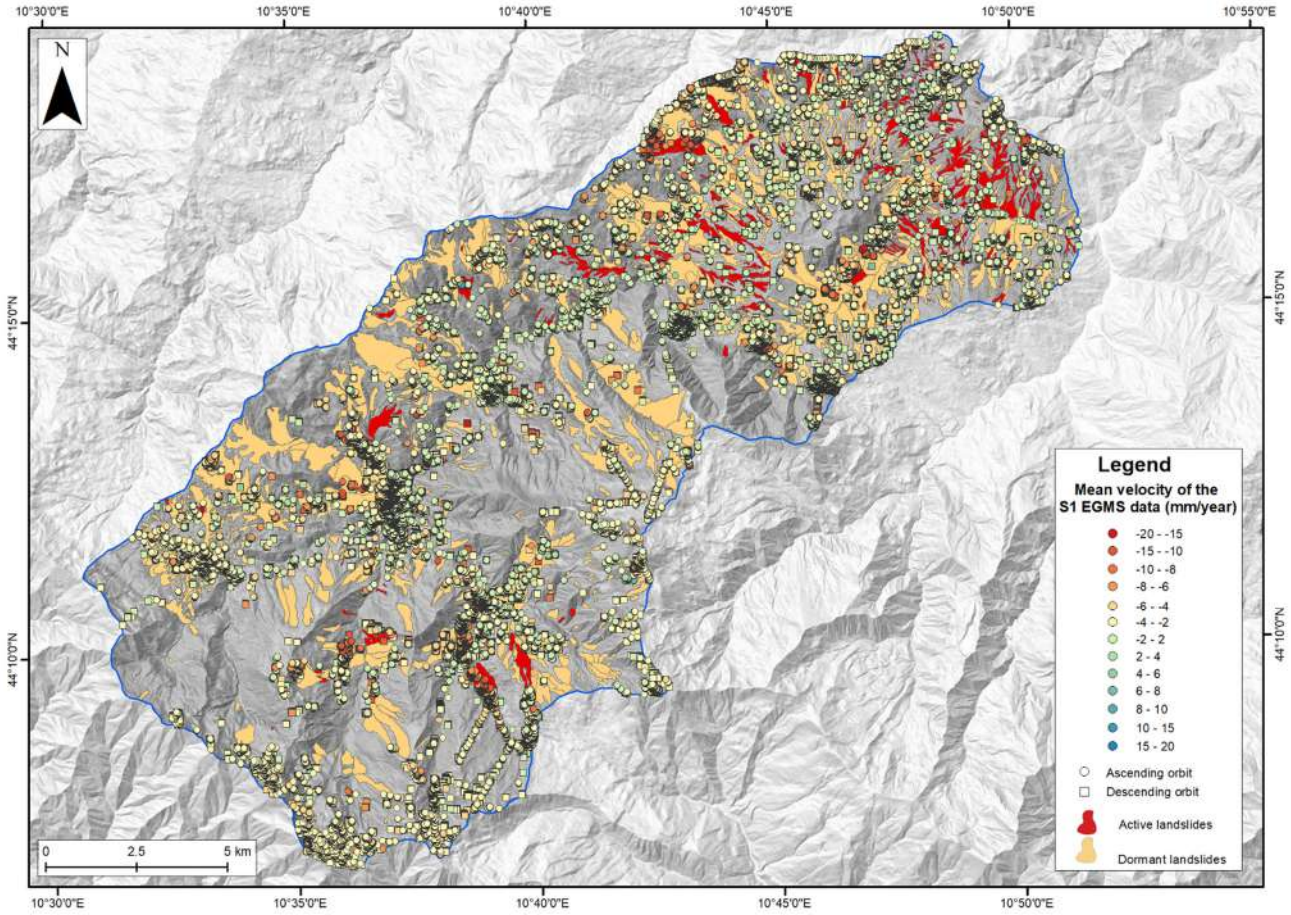

Figure 3. Sentinel-1 EGMS ascending and descending products over the Scoltenna Stream catchment (Modena Apennines, Italy) and landslides of the IFFI inventory.

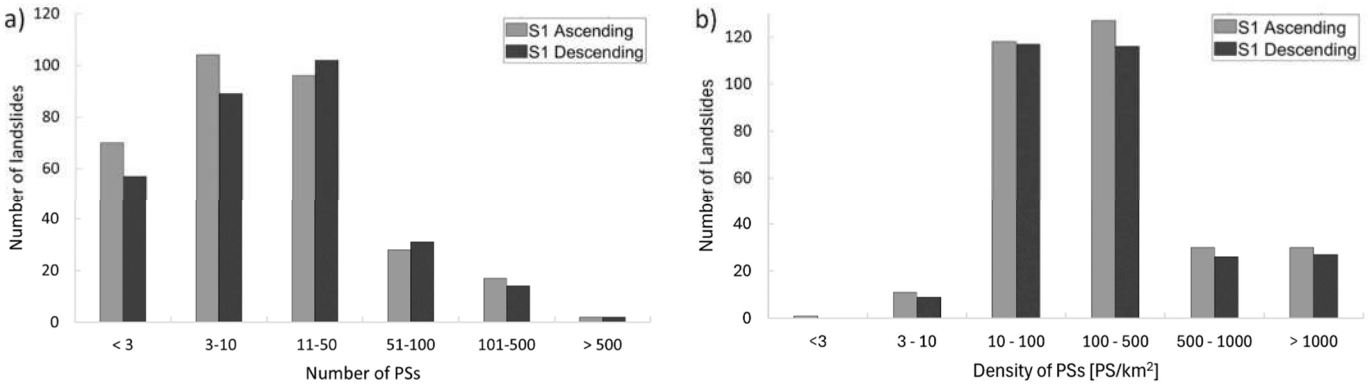

Figure 4. Results of Sentinel-1 EGMS ascending and descending data spatial analysis: (**a**) Range of PSs number and (**b**) Density of PSs inside the detected landslides.

Similarly, data from the descending orbit (Figure 3) overlap with 295 landslides, i.e., the 23.8% of the total mapped inside the catchment (1239), corresponding to the 58.0% of the catchment landslides area; the remaining 944 landslides (76.2%) are not represented. The 10.2% of the represented landslides (30 of the 295) are classified as active and the 89.8% (265) as dormant in the IFFI inventory. Moreover, 19.3% of the landslides include fewer than 3 PSs (57 of the 295), 30.3% contain 3 to 10 PSs (89 of the 265), 34.6% contain 11 to 50 PSs (102 of the 265), 10.5% contain 51 to 100 PSs (31 of the 265), 4.7% contain 101 to 500 PSs (14 of the 265), and only 0.6% are represented by more than 500 PSs (2 of 265) (Figure 4a). The distribution of the number of landslides with respect to the PSs density is presented in the graph of Figure 4b for both the S1 orbits, from which it can be noted that the majority of the detected landslides present a density of PSs in the ranges 10–100 PS/km^2 and 100–500 PS/km^2 for both the ascending and descending orbits.

The processing of the COSMO-SkyMed dataset from the ascending orbit (Figure 5) produced PSs that overlap with 140 landslides, corresponding to the 11.3% of the total number of landslides mapped within the Scoltenna catchment (1239). The other 88.7% of the landslides (1099) do not show corresponding PSs based on the processing of ascending COSMO-SkyMed data. The IFFI inventory classifies 14.3% of the landslides as active (20 of the 140) and the remaining 85.7% as dormant (120). The analysis of PS numerosity within the landslides' boundary shows 24.3% with fewer than 3 PSs (34 of the 140), 34.3% with 3 to 10 PSs (48 of the 140), 27.9% with 11 to 50 PSs (39 of the 140), 6.4% with 51 to 100 PSs (9 of the 140), 7.1% with 101 to 500 PSs (10 of the 140), and none including more than 500 PSs (Figure 6a).

PSs detected from the analysis of data collected along the descending orbit (Figure 5) relate to 162 landslides, corresponding to the 13.1% of the whole number of landslides (1239). As was also evidenced by results obtained from the ascending orbit, most of the landslides detected by descending orbit (1077) representing the 86.9% of the total have no corresponding PSs. In particular, the inventory classifies the 15.4% of the landslides as active (25 of the 162) and the 84.6% as dormant (137). The numerosity analysis shows 55.5% of the landslides including fewer than 3 PSs (90 of 162), 27.2% including 3 to 10 PSs (44 of the 162), 14.8% with 11 to 50 PSs (24 of the 162), 1.9% with 51 to 100 PSs (3 of the 162) and none of them with more than 500 PSs (Figure 6a). The distribution of the number of landslides with respect to the PSs density is presented in the graph of Figure 6b for both the CSK orbits. Most of the detected landslides present a density of PSs in the range 10–100 PS/km^2 and another consistent number of landslides have a density of 100–500 PS/km^2, for both the ascending and descending orbits.

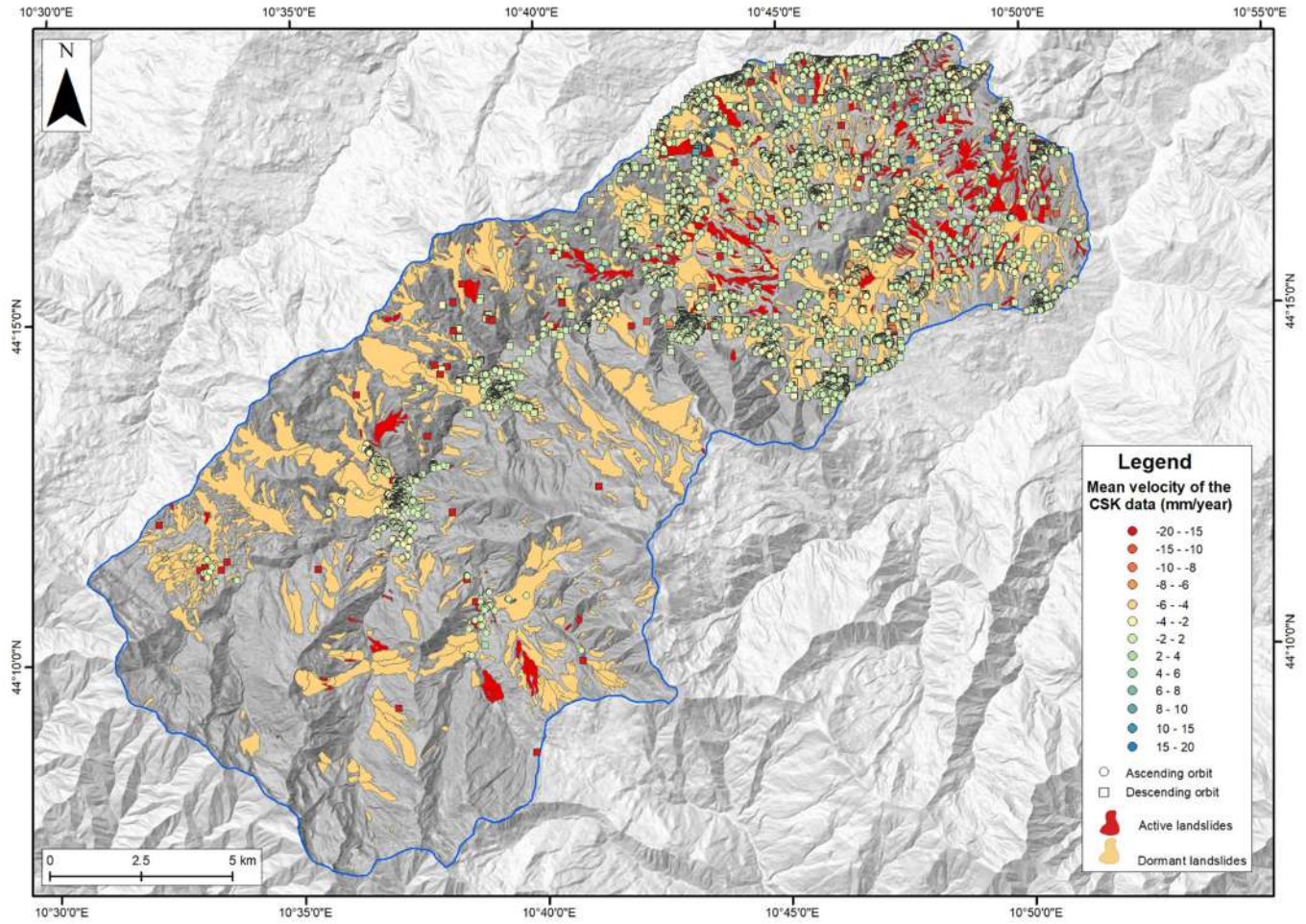

Figure 5. COSMO-SkyMed processing results from ascending and descending datasets over the Scoltenna Stream catchment (Modena Apennines, Italy) and landslides of the IFFI inventory.

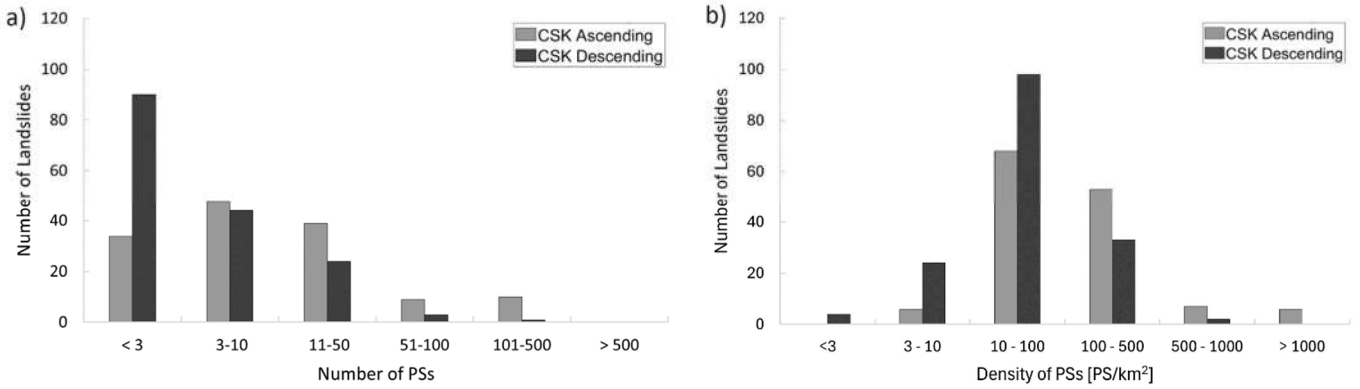

Figure 6. Results of COSMO-SkyMed ascending and descending data spatial analysis: (**a**) Range of PSs number and (**b**) Density of PSs inside the detected landslides.

To verify the consistency between the classification of landslides as provided by the IFFI inventory and the displacements available from the processing of SAR data, an analysis based on the PSs mean velocity has been conducted. For each landslide with a minimum of 3 PSs, the basic statistical parameters and their numerosity have been computed and distinguished between active and dormant landslides. Moreover, given the higher number of landslides detected by the EGMS S1 data in comparison to those detected by the CSK data, the outlined analysis was performed exclusively on the S1 data.

The results obtained are presented in Figures 7–10 for both the ascending and descending orbit. In the figures, the term "moving" landslide indicates landslides for which the sum between the mean of the PSs mean velocities and its standard deviation is greater than a selected threshold of 2 mm/year [81], given an accuracy of 1–2 mm/year of the multi-temporal techniques. Similarly, "non-moving" refers to landslides where such a term is less than 2 mm/year. In the figures, the ID used corresponds to the code reported in the attribute table of the shapefile containing all of the landslides located in the Emilia Romagna Region. The shapefile is provided by the Geoportale of Emilia Romagna Region (https://geoportale.regione.emilia-romagna.it/, accessed on 17 July 2024 [60]). Figures 7 and 8 represent the totality of the landslides detected during the ascending and descending satellite passes and classified by the IFFI inventory as active, while Figures 9 and 10 present only a subset of the landslides detected by both orbits classified as dormant due to the large number of them. The analysis of the totality of the detected dormant landslides is reported in the Supplementary Materials. Considering the active landslides detected by the S1 ascending data (Figure 7), 72% are classified as moving and 28% as non-moving; for the S1 descending data (Figure 8), 58.8% are classified as moving and 41.2% as non-moving. When the analysis of the dormant landslides is considered, for the S1 ascending data (Figure 9), 79.3% are moving and 20.7% are non-moving; for the S1 descending data (Figure 10), 54.3% are moving and 45.7% are non-moving. Along with the representation of the mean velocity and standard deviation, a pie chart presenting the global consistency between the IFFI classification and the SAR-based results is reported. The consistency between the IFFI classification and SAR results is verified whenever the sum of the mean velocity of the landslide and its standard deviation is greater than the selected threshold whereas the opposite holds for dormant landslides.

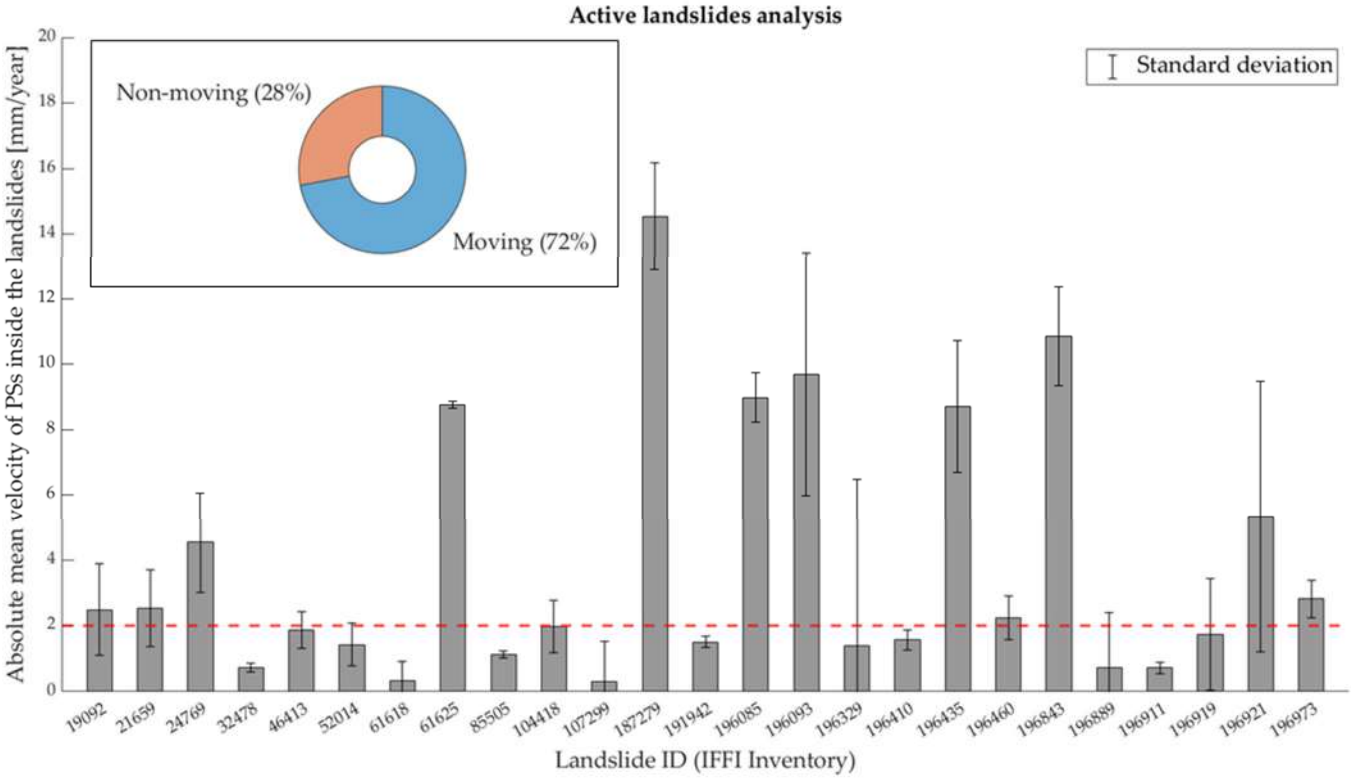

Figure 7. Analysis of the landslides' motion from ascending S1 EGMS data performed for landslides classified as active by the IFFI inventory.

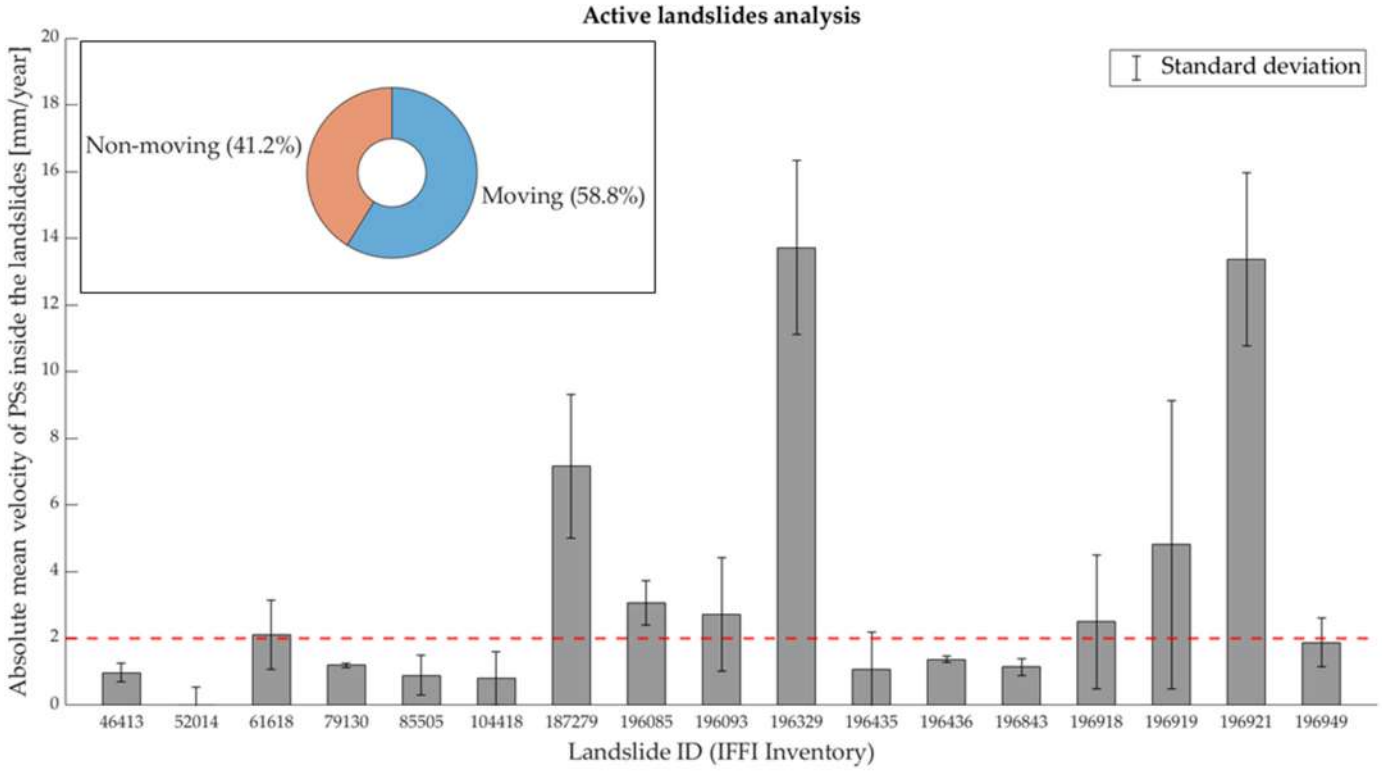

Figure 8. Analysis of the landslides' motion from descending S1 EGMS data performed for landslides classified as active by the IFFI inventory.

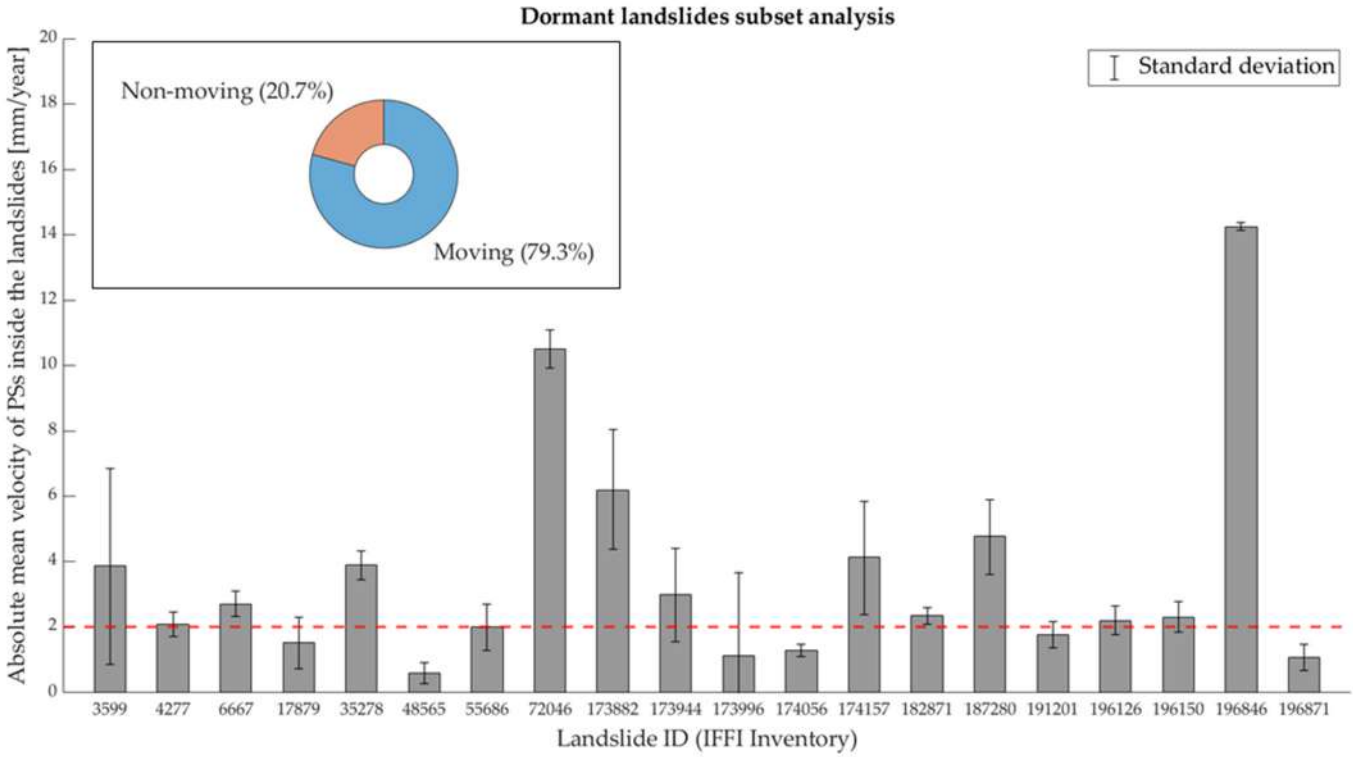

Figure 9. Analysis of the landslides' motion from ascending S1 EGMS data performed for a representative subset of landslides classified as dormant by the IFFI inventory. The totality of the analyzed landslides can be found in the Supplementary Materials.

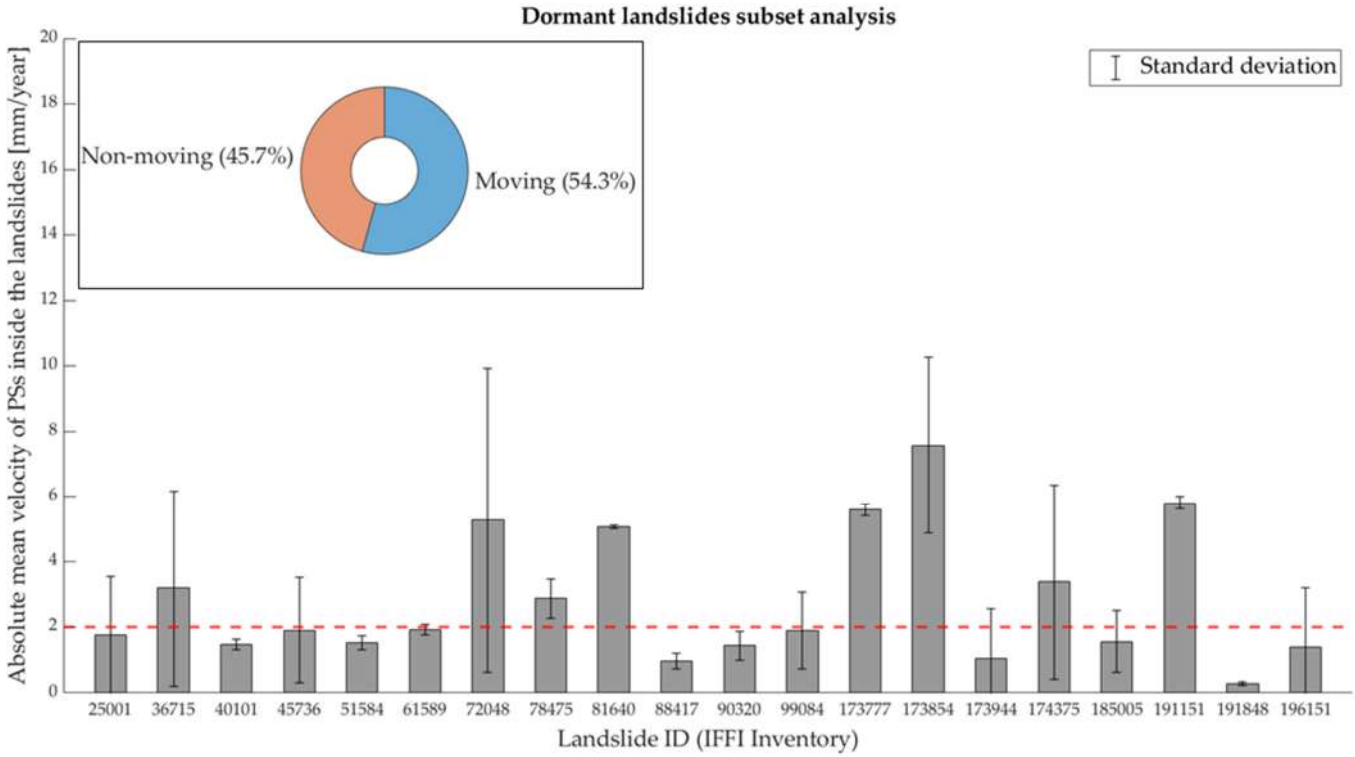

Figure 10. Analysis of the landslides' motion from S1 descending EGMS data performed for a representative subset of landslides classified as dormant by the IFFI inventory. The totality of the analyzed landslides can be found in the Supplementary Materials.

The results presented in Figures 7–10 have been mapped to provide a geographical representation of the achieved performances and possible responses linked to the main terrain properties, dominant coverages and slope exposure. Figures 11 and 12 show landslides classified according to the consistency between the IFFI inventory classification and the state of activity retrieved from the SAR ascending and descending data, respectively. The classification was performed according to five classes: landslides classified as active both by the IFFI inventory and the SAR state of activity, landslides classified as dormant both by the IFFI inventory and the SAR state of activity, landslides classified as active by the IFFI inventory and dormant by the SAR state of activity, landslides classified as dormant by the IFFI inventory and active by the SAR state of activity, and landslides non detected by SAR products (i.e., landslides for which fewer than 3 PSs have been detected).

To exemplify the multidisciplinary approach and to better demonstrate the potentialities of SAR interferometry for slow-moving landslide monitoring, in the following, a relevant case study is presented along with the obtained results. The proposed approach is specifically based on orthophoto visualization and geomorphological and satellite SAR analysis. More in detail, regarding the PS analysis, both the S1 and CSK data have been employed to perform a cross-validation between the datasets; moreover, a time series analysis has been conducted to monitor the landslide evolution through time.

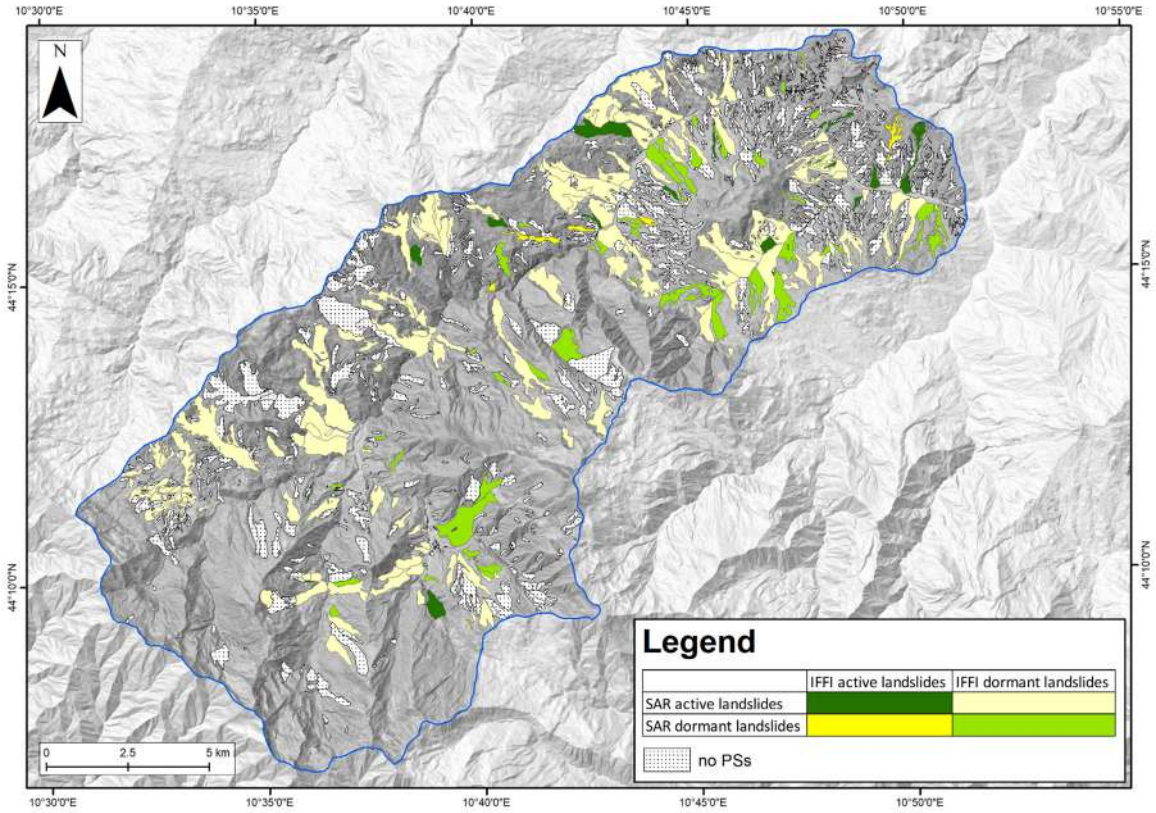

Figure 11. State of activity analysis of landslides by the IFFI inventory and the S1 EGMS ascending products.

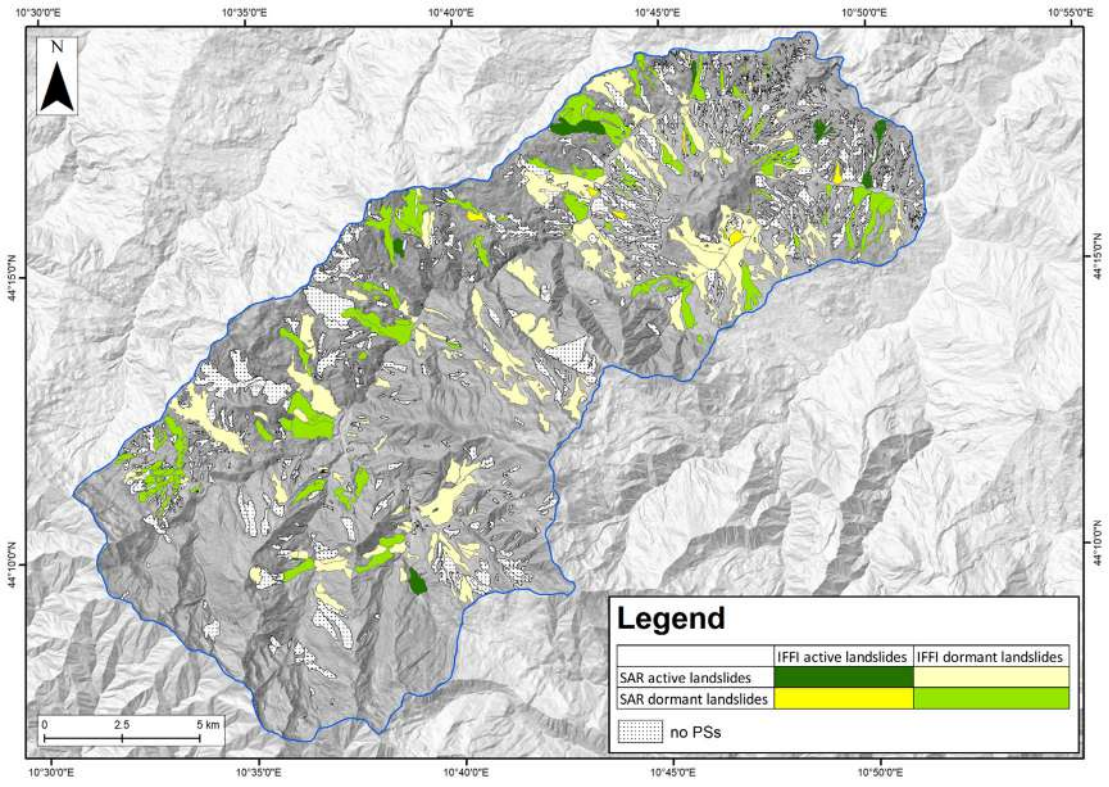

Figure 12. State of activity analysis of landslides by the IFFI inventory and the S1 EGMS descending products.

The Gaiato landslide, a 390,000 m^2 wide and 2.3 km long earth flow with an elevation difference of 540 m (see Figure 1 for the location of the landslide), has been chosen as the test site for the proposed methodology. The cross-validation between the independent SAR dataset considered in this work (i.e., S1 EGMS products and CSK data processed and calibrated by the authors) is presented. In particular, Figure 13 presents the extension of the landslides and the SAR products from the ascending and descending orbit for both satellites. As illustrated in the PSs maps of Figure 13, S1 data are more suited to describe the phenomenon occurring at the Gaiato landslide, particularly in vegetated areas, than CSK data. However, a comparison of the mean PSs velocities from the two datasets (considered independent from each other), performed as a cross-validation, demonstrated that both datasets can retrieve and describe the phenomenon as evidenced by the differences at the mm level in the mean velocity values. It is important to keep in mind that the S1 EGMS and CSK products were calibrated separately, following distinct procedures and exploiting different GNSS networks.

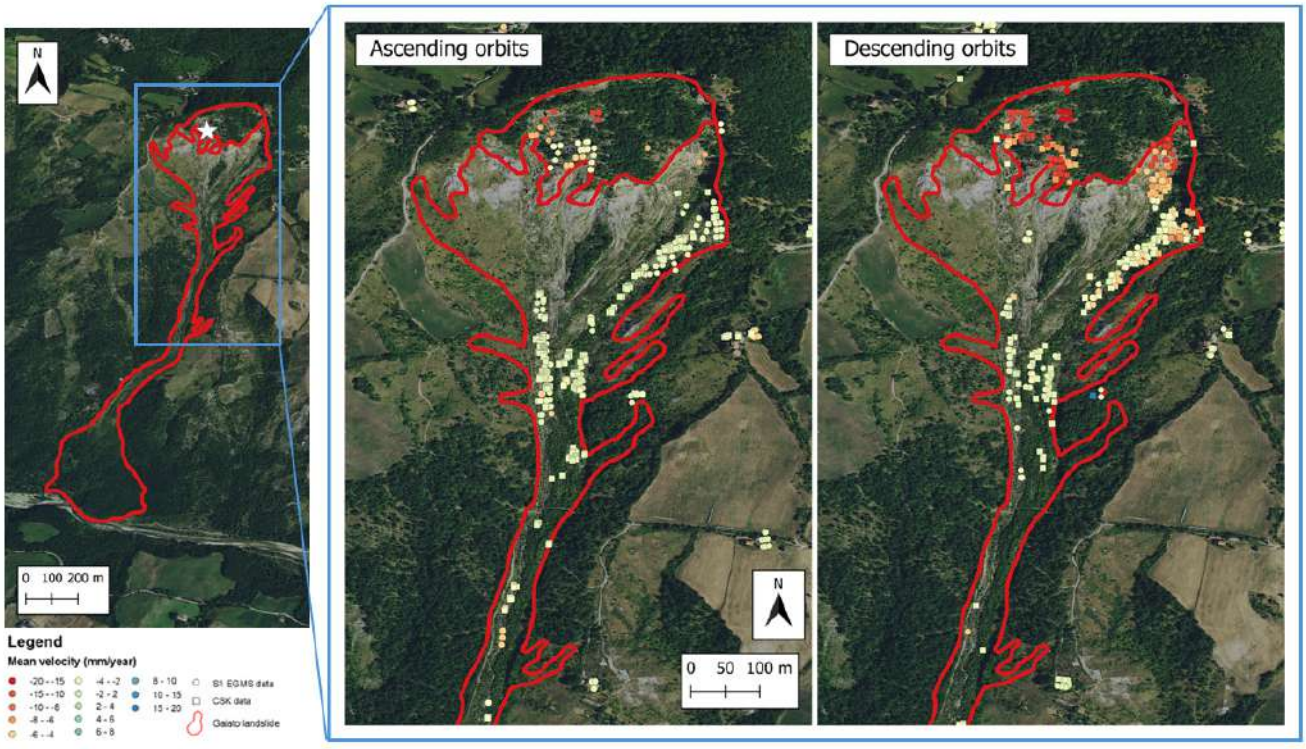

Figure 13. The extension of the Gaiato landslide (**left**); PSs from ascending S1 and CSK orbits (**center**); PSs from descending S1 and CSK orbits (**right**). The used orthophoto (year 2018) can be accessed through the Geoportal of the Emilia Romagna region (available online: https://geoportale.regione.emilia-romagna.it/, accessed on 17 July 2024). The white star indicates the point relevant to the successive time series analysis.

A deeper examination of the processes occurring at the Gaiato landslide was conducted by analyzing the time series of displacement of the selected PSs to monitor the evolution of the landslide over time. To this end, three independent datasets were considered: the S1 EGMS products, the CSK products processed by the authors (referring to the period 2012–2022) and the CSK products processed by the TRE Telerilevamento in the frame of the "Piano Straordinario di Telerilevamento" (PST), covering the period 2011–2014 (more information related to the PST can be found at [83]). In Figure 14, the time series of the three PSs nearest to the location identified by the white star of Figure 13 are presented. The point selected for subsequent time series analysis was identified as a key area of interest as it demonstrates the ability of the integrated method to study slow landslides and update the inventory. Indeed, the time series show that the area exhibits a well-defined deformative

trend and significative displacement values, with a slight increase of the mean velocity from the year 2018.

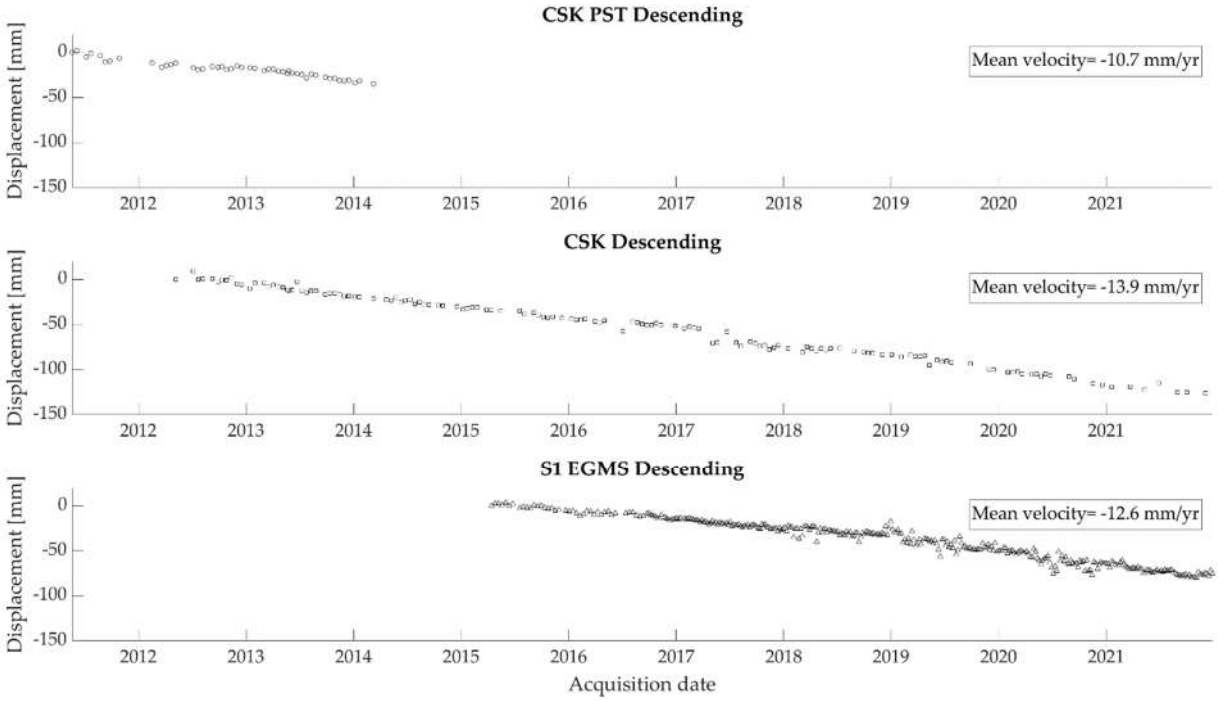

Figure 14. Time series of the 3 nearest PSs to the location identified by the white star of Figure 13. The time series of the CSK descending dataset from the "Piano Straordinario di Telerilevamento" [83] (**top**), the CSK descending dataset processed by the authors (**middle**), and the S1 EGMS descending products (**bottom**).

The multitemporal analysis comprised the mapping of the evolution of the extent of the Gaiato landslide, as observed through the orthophotos available from the Regional Web Map Service, and the changes in land use. The selected time span was aligned with the PSs time series.

In 2008, about half of the surface of the Gaiato landslide was covered by bare soil (56%) and the remaining part was covered in woods (32%), high density bushes (3%) and low density bushes (9%) (Figure 15a). In 2011, the woods and bushes increased: woods reached 41% of the surface, high density bushes 14%, and low density bushes 8%. Moreover, 12% of surface was covered by grass, leaving only 25% covered by bare soil (Figure 15b). In 2018, the grass increased (reaching 24% of the surface) at the expense of woods and low density bushes: 35% of the surface was covered by woods and 5% by low density bushes; the high density bushes maintained the same extension (14%) and the bare soil occupied 22% (Figure 15c). In 2020, the woods extension remained more or less stable (34%), while 16% of the surface was covered by high density bushes, 7% by low density bushes, 23% by grass, and bare soil decreased to 20% of the surface (Figure 15d). It can be observed that the vegetated areas in the upper part correspond to the calcarenite formations where the crown of the landslide is situated. Conversely, the bare soil, which makes the more active areas of the landslides easily recognizable, is concentrated in clay terrains, characterized by sparser bushes.

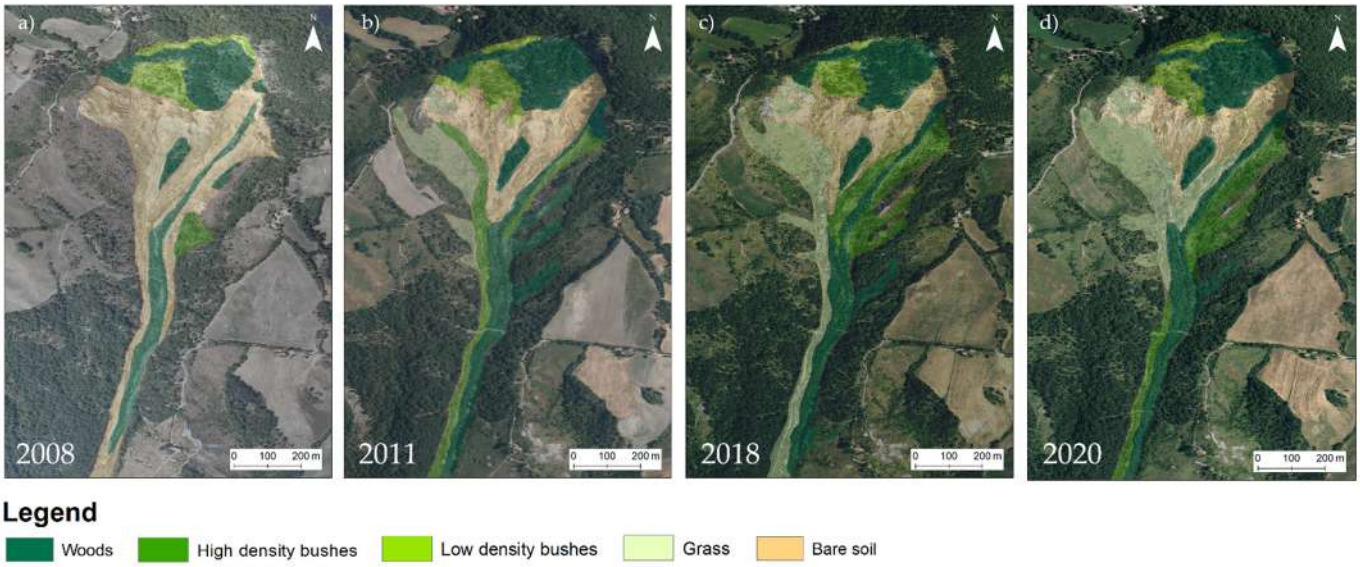

Figure 15. Evolution of the Gaiato landslide through time outlined by a comparison of orthophotos from 2008 (**a**), 2011 (**b**), 2018 (**c**), and 2020 (**d**).

5. Discussion

This research allowed us to assess the potential of multi-temporal SAR interferometry for the investigation of slow-moving landslides in the Scoltenna catchment (Northern Apennines, Italy). Specifically, the analysis of the dual-orbit (i.e., ascending and descending) and dual operational frequency C-band EGMS S1 and X-band CSK dataset processed by the authors over the study area enabled us to highlight the strengths and shortcomings of the use of PSI for such an investigation and to discuss the influence of the band of the signal and the geometry of acquisition on the obtained results.

The statistical analysis of the numerosity of PSs revealed that, despite the higher spatial resolution characterizing the CSK dataset, only 12% of the mapped landslides were detected using the CSK dataset compared to the 25% using S1 EGMS data. Furthermore, the enhanced sensitivity of the S1 data was also confirmed by the PS density analysis reported in Figures 4b and 6b, where a consistent number of landslides exhibited a density greater than 100 PS/km^2. The increased capability of the S1 C-band data to detect these phenomena could be due to its lower sensitivity to changes in vegetation covers during the investigated period and a short revisit time between acquisitions (6 days when the ensembled constellation of the S1A and S1B satellites is considered in comparison to the average 40 days of revisit time for the CSK dataset) (see Table 1). From the analysis of the PSs numerosity and density, it can be noted that the number of landslides detected by SAR is slightly different from ascending and descending geometry for the S1 and CSK datasets. The performance of the SAR data in detecting different slopes is mainly related to the acquisition geometry (i.e., the incidence and heading angle) of the orbit, the local topography, the steepness and aspect of the slope, the land cover, and its variation during the seasons. Consequently, the differences in the number of slopes detected by SAR data can be attributed to the orbit geometry. Some methodologies for the a priori estimation of the SAR orbits to landslide detection have been recently proposed to provide preliminary knowledge on the suitability of the selected dataset for a specific area before the processing of a large amount of data [84–86].

In view of the better suitability shown by C-band data for the purposes of this research, the following analysis, oriented to the study of the state of the activity of the landslide, was performed for S1 data only. The choice of a minimum number of 3 PSs allowed poorly represented landslides (22% of the S1 ascending data and 19% of the S1 descending data) to be ignored. The combination of mean velocity and standard deviation (Figures 7–10) allowed validation of the active and dormant landslides (as indicated by the IFFI landslide

inventory) by dual information derived from the ascending and descending datasets. Moreover, the use of the standard deviation for landslides with a consistent number of targets could inform on the variability and the spatial distribution of the phenomenon, providing useful information for detailed geomorphological analysis. Figures 7 and 8 indicate that for landslides classified as active by the IFFI inventory (approximately the 10% of the landslides detected by the EGMS S1 dataset) there is substantial consistency with the SAR-based results reported in the present work. This is also evidenced by a majority of landslides classified as a "moving landslide" after the analysis of the SAR data (72% and 59% for ascending and descending orbits, respectively). When considering the landslides classified as dormant by the IFFI inventory, the percentage of consistency between the IFFI and the SAR-based classification was lower. Approximately only the 28% and 46% of the dormant landslides for the ascending and descending orbits, respectively, were classified by the proposed method as "non-moving". These results have been mapped and are presented in Figures 11 and 12, where another important clue on the potential of SAR to update the inventory is offered as it is clear that the majority of "non agreement" between the two states of activity classifications are related to cases in which landslides are classified as dormant by the IFFI inventory.

The presented results allow us to critically discuss the ability of SAR interferometry in the update of landslides inventory. In particular, it is demonstrated that the multi-temporal interferometric technique is not fully capable of detecting slope deformations in the Scoltenna catchment, as only a fraction of the totality of landslides mapped by the IFFI inventory were detected. However, when the total landslide area of the catchment is considered, we demonstrated that the combination of the S1 EGMS ascending and descending products allowed for the detection of 62.8% of the landslide area. This can be also noted from Figures 11 and 12, which show that, as a great number of very small landslides have not been detected by SAR products, the mere counting of the number of detected landslides is not representative of the method's potential. This is verified in areas characterized by very small and distributed phenomena, such as the Northern Apennines. Therefore, the obtained results related to the high landside area coverage by SAR data prove that the potential of the proposed method for the investigation of slow-moving landslides at the basin scale and toward the semi-automated update of part of the landslide inventory is still worth noting. Indeed, the updating of the landslide inventories could represent a very challenging task due to the large amount of manual work required, in particular after extreme events that could trigger new phenomena or reactivate dormant landslides. Automated or semi-automated methods to accomplish, in a complete and reliable way, the aforementioned task would be very helpful [82]. Although methods based on multi-temporal interferometry have already been proposed by a limited number of papers [81,87], one of the innovations introduced by the present work is related to its contribution to the exploration and exploitation of the potential offered by the new EGMS products.

The potential of the multidisciplinary approach using SAR data and geomorphological analysis were further described for the case study represented by the Gaiato landslide. The analyses carried out on the selected test site allowed three main objectives, along with their novel features, to be achieved. The first was the cross-validation of SAR data from sensors operating at different frequencies (i.e., S1 EGMS products and CSK products processed for this research by the authors), from which it was found that differences of a few millimeters could be observed between the independent datasets. Secondly, the relevance of an integrated approach for the update of a landslide inventory has been demonstrated, proving that the proposed methodology is able to effectively retrieve crucial insights into the mapping, state of activity, and evolution of slow-moving landslides. The Gaiato landslide proved to be a relevant example in the updating of the IFFI inventory (updated to the year 2016 for the Emilia-Romagna region) and, in particular, for a deeper understanding of the temporal and spatial evolution of the phenomenon. In fact, the joint analysis of time series of displacements and orthophotos shows that, in recent years, the landslide experienced a faster evolution, as the mean velocity increased and the extent of

the grass and bare soil increased at the expense of woods and bushes. Finally, an update of the SAR products already available for the area is offered. Indeed, the series of CSK data from the PST, which partially overlaps with the proposed CSK processing, ends at the beginning of 2014; therefore, the CSK processing by the authors offers a solution to fill the gap between the time series of the PST and the EGMS products, allowing for a seamless displacement analysis in the area from 2011 to 2022.

However, limitations in the use of MT-InSAR to update landslide inventories over poorly urbanized areas have to be emphasized. Phenomena that are too fast to be revealed by C-band data would not be correctly retrieved. In this regard, the perspectives offered by L-band SAR systems require deeper considerations as a longer signal wavelength leads to greater penetration through vegetation cover, higher coherence between image pairs, and an increased ability to detect faster displacement. Special attention should be paid to recent or expected satellite missions designed to acquire SAR data. Among these, the Satélite Argentino de Observación con Microondas (SAOCOM) L-band full-polarimetric constellation by the National Commission for Space Activities of Argentina (CONAE) could be mentioned [88,89]. It comprises two twin radar satellites operating with a revisiting time of 8 days and good spatial resolution (10 m $\times$ 10 m in the range and azimuth directions). In addition, the planned ESA L-band SAR mission named Radar Observing System for Europe (ROSE-L), expected to be launched in 2028, will ensure an enhanced continuity with the S1 constellation (along with the S1 Next Generation) in the slope deformation monitoring by using the same acquisition mode (S1 Interferometric Wide swath mode) [90]. In light of the mentioned advantages and drawbacks of the use of the different data at different bands, it is important to highlight that these data could be employed in a synergistic way to overcome the limitations given by the use of a single band. Besides the SAR data employed in the analysis, multi-temporal interferometric techniques demonstrated the ability to provide accurate data for monitoring surface deformations and, in particular, applying it to a study area prone to landslides as the one object of the present study. They can yield valuable insights into the dynamics of slope instability and the efficiency of this advanced technology.

6. Conclusions

The integration and synergy among geomorphological analyses, field surveys, ground truthing and Earth Observation-based techniques are useful to detect and monitor slope deformations at a basin scale. Among the techniques that can provide accurate measurements of ground displacements, multi-temporal synthetic aperture radar data is able to achieve a millimeter-scale accuracy. This research investigated the potential of multi-temporal SAR interferometry in a slow-moving landslide study area, the Scoltenna catchment in the Northern Apennines (Italy). Furthermore, the use of data from dual-orbit Sentinel-1 C-band and COSMO-SkyMed X-band systems enabled the assessment of the influence of the signal frequency and the acquisition geometry on the number of detected landslides and on the density of the permanent targets. Regardless of the limitations of the multi-temporal interferometric techniques, the results achieved demonstrated that the C-band systems have an enhanced ability to detect and describe the phenomena considering both the number of landslides and the PS density; in fact, exploiting the EGMS S1 dataset, almost 63% of the landslide areas mapped within the inventory have been detected and the PS density exceeded the 100 PS/km^2 for a consistent number of landslides. Another aim of the presented work was the evaluation of the landslide state of activity with the multi-temporal SAR technique; this was achieved by retrieving the mean velocity and its standard deviation for each of the detected landslides from the S1 EGMS products. State of activity results by SAR were compared with those from the available inventory. The statistical analysis demonstrated that the proposed approach could be considered a viable solution for the exploitation of EGMS projects in the update of the landslide inventory. In particular, this research provides useful updates of the state of activity of the IFFI inventory for each landslide inside the Scoltenna catchment detected for at least one orbit of the S1

EGMS dataset, verifying the consistency between the inventory and the SAR results. The synergistic use of SAR, optical data, and geomorphological analysis demonstrated the capabilities of the proposed approach in updating the mapping and state of activity of the Gaiato landslide, a relevant phenomenon inside the study area.

To enhance the number of detected landslides and the reliability of the proposed analysis, the use of satellite data at a lower frequency is advised; in this scenario, the L-band SAOCOM and ROSE-L constellations could offer new perspectives in the investigation of a slow-moving landslide field. These data, coupled with field inspections, could be employed in a synergistic way to overcome the limitations of the use of a single method to allow an automatic update of landslide inventories.

Supplementary Materials: The following supporting information can be downloaded at: https://www.mdpi.com/article/10.3390/land13091505/s1, Figure S1: Dormant landslides analysis—Ascending orbit; Figure S2: Dormant landslides analysis—Descending orbit; Table S1: IFFI inventory links.

Author Contributions: Conceptualization, C.P., F.G., P.R., M.S. and F.M.; methodology, C.P., F.G., P.R. and F.M.; software, C.P., F.G. and F.M.; validation, C.P., F.G. and F.M.; formal analysis, C.P., F.G., P.R. and F.M.; investigation, C.P., F.G., P.R., M.S. and F.M.; resources, C.P., F.G., P.R. and F.M.; data curation, C.P., F.G. and F.M.; writing—original draft preparation, C.P., F.G., P.R. and F.M.; writing—review and editing, C.P., F.G., P.R., M.S. and F.M.; visualization, C.P., F.G., P.R., M.S. and F.M.; supervision, M.S. and F.M.; project administration, M.S., E.P. and F.M.; funding acquisition, M.S., E.P. and F.M. All authors have read and agreed to the published version of the manuscript.

Funding: This research was funded by the Unimore Interdisciplinary Research Project "Deciphering the response of the slope-fluvial system to environmental changes: Toward effective forecasting and Prevention of hydrogeological RIsks in the Modena Apennines (PRIMA)"—Fondo di Ateneo per la Ricerca 2023—Linea FOMO (CUP E93C23002210007). This research has also been carried out within the framework of the collaboration between the Inter-Departmental Research and Innovation Centre on Constructions and Environmental Services (CRICT) of the University of Modena and Reggio Emilia and the Regional Agency for Territorial Safety and Civil Protection of Emilia-Romagna, in the frame of the project "Analysis of the interaction between fluvial dynamics and slope processes aiming at the recognition of geomorphological risk situations" (0277490).

Data Availability Statement: This publication has been prepared using European Union's Copernicus Land Monitoring Service information: https://doi.org/10.2909/d92e61be-d6e8-4bc1-aa10-f742bf27bab9 (accessed on 17 July 2024). The EGMS S1 data presented in the study are openly available at https://egms.land.copernicus.eu/ (accessed on 17 July 2024). The COSMO-SkyMed Products by the Italian Space Agency (ASI), processed during the preparation of this work, were delivered under a license to use by ASI. The data from the Piano Straordinario di Teleriveamento (PST) processed during the preparation of this work, can be requested to the Geoportale Nazionale (https://gn.mase.gov.it/portale/distribuzione-dati-pst?p_l_back_url=%2Fportale%2Fricerca%3Fr%3Dcitazione%252B; accessed on 17 July 2024).

Acknowledgments: The authors are grateful to the Regional Agency for Territorial Safety and Civil Protection of Emilia-Romagna, namely to Francesca Lugli for the technical assistance and support.

Conflicts of Interest: The authors declare no conflicts of interest.

References

1. Cruden, D.M.; Varnes, D.J. Landslide Types and Processes. *Transp. Res. Board Spec. Rep.* **1996**, *247*, 36–75.
2. Tzouvaras, M.; Danezis, C.; Hadjimitsis, D.G. Differential SAR Interferometry Using Sentinel-1 Imagery-Limitations in Monitoring Fast Moving Landslides: The Case Study of Cyprus. *Geosciences* **2020**, *10*, 236. [CrossRef]
3. Song, C.; Yu, C.; Li, Z.; Utili, S.; Frattini, P.; Crosta, G.; Peng, J. Triggering and recovery of earthquake accelerated landslides in Central Italy revealed by satellite radar observations. *Nat. Commun.* **2022**, *13*, 7278. [CrossRef] [PubMed]
4. Galloway, W. The landslide in the Rhymney valley. *Nature* **1906**, *73*, 425–426. [CrossRef]
5. Lu, C.; Chan, Y.; Hu, J.; Chiu, C.; Chu, C.; Tseng, C.; Chang, C. Velocity distribution and movement of multiple slow-moving landslides characterized by an optimized MTInSAR workflow. *Eng. Geol.* **2023**, *327*, 107339. [CrossRef]
6. Mainsant, G.; Larose, G.; Brönnimann, C.; Jongmans, D.; Michoud, C.; Jaboyedoff, M. Ambient seismic noise monitoring of a clay landslide: Toward failure prediction. *J. Geophys. Res. Earth Surf.* **2012**, *117*, F01030. [CrossRef]

7. Schulz, W.H.; Smith, J.B.; Wang, G.; Jiang, Y.; Roering, J.J. Clayey landslide initiation and acceleration strongly modulated by soil swelling. *Geophys. Res. Lett.* **2018**, *45*, 1888–1896. [CrossRef]
8. Lacroix, P.; Handwerger, A.L.; Bièvre, G. Life and death of slow-moving landslides. *Nat. Rev. Earth Environ.* **2020**, *1*, 404–419. [CrossRef]
9. Li, Y.; Utili, S.; Milledge, D.; Chen, L.; Yin, K. Chasing a complete understanding of the failure mechanisms and potential hazards of the slow moving Liangshuijing landslide. *Eng. Geol.* **2021**, *281*, 105977. [CrossRef]
10. Borrelli, L.; Nicodemo, G.; Ferlisi, S.; Peduto, D.; Di Nocera, S.; Gullà, G. Geology, slow-moving landslides, and damages to buildings in the Verbicaro area (north-western Calabria region, southern Italy). *J. Maps* **2018**, *14*, 32–44. [CrossRef]
11. Zhang, Y.; Meng, X.; Jordan, C.; Novellino, A.; Dijkstra, T.; Chen, G. Investigating slow-moving landslides in the Zhouqu region of China using InSAR time series. *Landslides* **2018**, *15*, 1299–1315. [CrossRef]
12. Guzzetti, F.; Mondini, A.C.; Cardinali, M.; Fiorucci, F.; Santangelo, M.; Chang, K.-T. Landslide inventory maps: New tools for an old problem. *Earth-Sci. Rev.* **2012**, *112*, 42–66. [CrossRef]
13. Parise, M.; Coe, J.A.; Savage, W.Z.; Varnes, D.J. The Slumgullion landslide (southwestern Colorado, USA): Investigation and monitoring. In Proceedings of the International Conference FLOWS, Sorrento, Italy, 22–27 September 2003; pp. 11–13.
14. Macfarlane, D.F. Observations and predictions of the behavior of large, slow-moving landslides in schist, Clyde Dam reservoir, New Zealand. *Eng. Geol.* **2009**, *109*, 5–15. [CrossRef]
15. Kavoura, K.; Konstantopoulou, M.; Depountis, N.; Sabatakakis, N. Slow-moving landslides: Kinematic analysis and movement evolution modeling. *Environ. Earth Sci.* **2020**, *79*, 1–11. [CrossRef]
16. Mora, O.E.; Lenzano, M.G.; Toth, C.K.; Grejner-Brzezinska, D.A.; Fayne, J.V. Landslide Change Detection Based on Multi-Temporal Airborne LiDAR-Derived DEMs. *Geosciences* **2018**, *8*, 23. [CrossRef]
17. Azmoon, B.; Biniyaz, A.; Liu, Z. Use of High-Resolution Multi-Temporal DEM Data for Landslide Detection. *Geosciences* **2022**, *12*, 378. [CrossRef]
18. Tomás, R.; Li, Z.; Lopez-Sanchez, J.M.; Liu, P.; Singleton, A. Using wavelet tools to analyse seasonal variations from InSAR time-series data: A case study of the Huangtupo landslide. *Landslides* **2016**, *13*, 437–450. [CrossRef]
19. Bounab, A.; El Kharim, Y.; El Hamdouni, R.; Hlila, R. A multidisciplinary approach to study slope instability in the Alboran Sea shoreline: Study of the Tamegaret deep-seated slow-moving landslide in Northern Morocco. *J. Afr. Earth Sci.* **2021**, *184*, 104345. [CrossRef]
20. Dille, A.; Kervyn, F.; Handwerger, A.L.; d'Oreye, N.; Derauw, D.; Mugaruka Bibentyo, T.; Samsonov, S.; Malet, J.-P.; Kervyn, M.; Dewitte, O. When image correlation is needed: Unravelling the complex dynamics of a slow-moving landslide in the tropics with dense radar and optical time series. *Remote Sens. Environ.* **2021**, *258*, 112402. [CrossRef]
21. Parenti, C.; Rossi, P.; Mancini, F.; Scorpio, V.; Grassi, F.; Ciccarese, G.; Lugli, F.; Soldati, M. Multitemporal Analysis of Slow-Moving Landslides and Channel Dynamics through Integrated Remote Sensing and In Situ Techniques. *Remote Sens.* **2023**, *15*, 3563. [CrossRef]
22. Ciccarese, G.; Tondo, M.; Mulas, M.; Bertolini, G.; Corsini, A. Rapid Assessment of Landslide Dynamics by UAV-RTK Repeated Surveys Using Ground Targets: The Ca' Lita Landslide (Northern Apennines, Italy). *Remote Sens.* **2024**, *16*, 1032. [CrossRef]
23. Van Wyk de Vries, M.; Arrell, K.; Basyal, G.K.; Densmore, A.L.; Dunant, A.; Harvey, E.L.; Jimee, G.K.; Kincey, M.E.; Li, S.; Singh Pujara, D.; et al. Detection of slow-moving landslides through automated monitoring of surface deformation using Sentinel-2 satellite imagery. *Earth Surf. Process. Landf.* **2024**, *49*, 1241–1482. [CrossRef]
24. Savvaidis, P.D. Existing Landslide Monitoring Systems and Techniques. In *From Stars to Earth and Culture*; School of Rural and Surveying Engineering, Aristotle University of Thessaloniki: Thessaloniki, Greece, 2003; pp. 242–258.
25. Strozzi, T.; Farina, P.; Corsini, A.; Ambrosi, C.; Thüring, M.; Zilger, J.; Wiesmann, A.; Wegmüller, U.; Werner, C. Survey and monitoring of landslide displacements by means of L-band satellite SAR interferometry. *Landslides* **2005**, *2*, 193–201. [CrossRef]
26. Bayer, B.; Simoni, A.; Mulas, M.; Corsini, A.; Schmidt, D. Deformation responses of slow moving landslides to seasonal rainfall in the Northern Apennines, measured by InSAR. *Geomorphology* **2018**, *308*, 293–306. [CrossRef]
27. Mulas, M.; Formicola, P.; Corsini, A. Development of GNSS LOwCOst receivers based monitoring array for landslides continuous monitoring. *Geophys. Res. Abstr.* **2018**, *20*, 18048.
28. Lissak, C.; Bartsch, A.; De Michele, M.; Gomez, C.; Maquaire, O.; Raucoules, D.; Roulland, T. Remote Sensing for Assessing Landslides and Associated Hazards. *Surv. Geophys.* **2020**, *41*, 1391–1435. [CrossRef]
29. Parenti, C.; Rossi, P.; Soldati, M.; Grassi, F.; Mancini, F. Integrated Geomatics Surveying and Data Management in the Investigation of Slope and Fluvial Dynamics. *Geosciences* **2022**, *12*, 293. [CrossRef]
30. Massonnet, D.; Feigl, K.L. Discrimination of geophysical phenomena in satellite radar interferograms. *Geophys. Res. Lett.* **1995**, *22*, 1537–1540. [CrossRef]
31. Gabriel, A.K.; Goldstein, R.M.; Zebker, H.A. Mapping small elevation changes over large areas: Differential radar interferometry. *J. Geophys. Res. Solid Earth* **1989**, *94*, 9183–9191. [CrossRef]
32. Kimura, H.; Yamaguchi, Y. Detection of landslide areas using satellite radar interferometry. *Photogramm. Eng. Remote Sens.* **2000**, *66*, 337–344.
33. Ferretti, A.; Prati, C.; Rocca, F. Permanent scatterers in SAR interferometry. *IEEE Trans. Geosci. Remote Sens.* **2001**, *39*, 8–20. [CrossRef]

34. Berardino, P.; Fornaro, G.; Lanari, R.; Sansosti, E. A new algorithm for surface deformation monitoring based on small baseline differential SAR interferograms. *IEEE Trans. Geosci. Remote Sens.* **2002**, *40*, 2375–2383. [CrossRef]
35. Hooper, A.; Zebker, H.; Segall, P.; Kampes, B. A new method formeasuring deformation on volcanoes and other natural terrains using InSAR persistent scatterers. *Geophys. Res. Lett.* **2004**, *31*, L23611. [CrossRef]
36. Ferretti, A.; Fumagalli, A.; Novali, F.; Prati, C.; Rocca, F.; Rucci, A. A New Algorithm for Processing Interferometric Data-Stacks: SqueeSAR. *IEEE Trans. Geosci. Remote Sens.* **2011**, *49*, 3460–3470. [CrossRef]
37. Casu, F.; Manzo, M.; Lanari, R. A quantitative assessment of the SBAS algorithm performance for surface deformation retrieval from DInSAR data. *Remote Sens. Environ.* **2006**, *102*, 195–210. [CrossRef]
38. Cigna, F.; Tapete, D.; Casagli, N. Semi-automated extraction of Deviation Indexes (DI) from satellite Persistent Scatterers time series: Tests on sedimentary volcanism and tectonically-induced motions. *Nonlinear Process. Geophys.* **2012**, *19*, 643–655. [CrossRef]
39. Berti, M.; Corsini, A.; Franceschini, S.; Iannacone, J.P. Automated classification of Persistent Scatterers Interferometry time series. *Nat. Hazards Earth Syst. Sci.* **2013**, *13*, 1945–1958. [CrossRef]
40. Wasowski, J.; Bovenga, F. Investigating landslides and unstable slopes with satellite Multi Temporal Interferometry: Current issues and future perspectives. *Eng. Geol.* **2014**, *174*, 103–138. [CrossRef]
41. Mantovani, M.; Devoto, S.; Piacentini, D.; Prampolini, M.; Soldati, M.; Pasuto, A. Advanced SAR Interferometric Analysis to Support Geomorphological Interpretation of Slow-Moving Coastal Landslides (Malta, Mediterranean Sea). *Remote Sens.* **2016**, *8*, 443. [CrossRef]
42. Raspini, F.; Bianchini, S.; Ciampalini, A.; Del Soldato, M.; Montalti, R.; Solari, L.; Tofani, V.; Casagli, N. Persistent scatterers continuous streaming for landslide monitoring and mapping: The case of the Tuscany region (Italy). *Landslides* **2019**, *16*, 2033–2044. [CrossRef]
43. Solari, L.; Del Soldato, M.; Raspini, F.; Barra, A.; Bianchini, S.; Confuorto, P.; Casagli, N.; Crosetto, M. Review of satellite interferometry for landslide detection in Italy. *Remote Sens.* **2020**, *12*, 1351. [CrossRef]
44. Duro, J.; Sabater, J.R.; Albiol, D.; Koudogbo, F.N.; Arnaud, A. Comparative analyses of multi-frequency PSI ground deformation measurements. In Proceedings of the Fringe, Frascati, Italy, 19–23 September 2011; pp. 19–23.
45. Hensley, S.; Van Zyl, J.; Lavalle, M.; Neumann, M.; Michel, T.; Muellerschoen, R.; Pinto, N.; Simard, M.; Moghaddam, M. L-Band and P-Band Studies of Vegetation at JPL. In Proceedings of the 2015 IEEE Radar Conference, Johannesburg, South Africa, 27–30 October 2015; IEEE: Piscataway, NJ, USA, 2015; pp. 516–520. [CrossRef]
46. Schlögel, R.; Malet, J.-P.; Doubre, C.; Lebourg, T. Structural Control on the Kinematics of the Deep-Seated La Clapière Landslide Revealed by L-Band InSAR Observations. *Landslides* **2016**, *13*, 1005–1018. [CrossRef]
47. Inventario dei Fenomeni Franosi in Italia. Available online: https://idrogeo.isprambiente.it/app/iffi (accessed on 16 May 2024).
48. Bettelli, G.; De Nardo, M.T. Geological Outlines of the Emilia Apennines (Northern Italy) and Introduction to the Formations Surrounding the Landslides which Resumed Activity in the 1994–1999 period. *Quad. Geol. Appl.* **2001**, *8*, 1–26.
49. Cerrina Feroni, A.; Martelli, L.; Martinelli, P.; Ottria, G.; Catanzariti, R. Carta Geologico-Strutturale dell'Appennino Emiliano-Romagnolo alla Scala 1:250,000, (Regione Emilia-Romagna, Servizio Geologico, Sismico e dei Suoli, CNR, Istituto di Geoscienze e Georisorse, Pisa), S.EL.CA. Firenze. 2002. Available online: https://geodata.mit.edu/catalog/mit-q2c4ny27r5jey (accessed on 11 March 2023).
50. Bertolini, G.; Canuti, P.; Casagli, N.; De Nardo, M.T.; Egidi, D.; Mainetti, M.; Pignone, R.; Pizziolo, M. *Carta della Pericolosità Relativa da Frana della Regione Emilia-Romagna*; SystemCart: Rome, Italy, 2002.
51. Bertolini, G.; Guida, M.; Pizziolo, M. Landslides in Emilia-Romagna region (Italy): Strategies for Hazard Assessment and Risk Management. *Landslides* **2005**, *2*, 302–312. [CrossRef]
52. Bertolini, G.; Pizziolo, M. Risk assessment strategies for the reactivation of earth flows in the Northern Apennines (Italy). *Eng. Geol.* **2008**, *102*, 3–4. [CrossRef]
53. Chelli, A.; Francese, R.; Petrella, E.; Carri, A.; Quagliarini, A.; Segalini, A.; Caporicci, M.P.; Diena, M.; Giorgi, M.; Celico, F. A multi-parameter field monitoring system to investigate the dynamics of large earth slides–earth flows in the Northern Apennines, Italy. *Eng. Geol.* **2020**, *275*, 105780. [CrossRef]
54. Ronchetti, F.; Borgatti, L.; Cervi, F.; Lucente, C.C.; Veneziano, M.; Corsini, A. The Valoria Landslide Reactivation in 2005–2006 (Northern Apennines, Italy). *Landslides* **2007**, *4*, 189–195. [CrossRef]
55. Trigila, A.; Iadanza, C.; Bussettini, M.; Lastoria, B.; Barbano, A.; Munafò, M. Dissesto Idrogeologico in Italia: Pericolosità e Indicatori di Rischio. *Rapporto* **2015**, *233*, 2015.
56. Bertolini, G.; Corsini, A.; Tellini, C. Fingerprints of Large-Scale Landslides in the Landscape of the Emilia Apennines. In *Landscapes and Landforms of Italy. World Geomorphological Landscapes*; Soldati, M., Marchetti, M., Eds.; Springer: Cham, Switzerland, 2017; pp. 215–224. [CrossRef]
57. Mulas, M.; Ciccarese, G.; Ronchetti, F.; Truffelli, G.; Corsini, A. Slope Dynamics and Streambed Uplift during the Pergalla Landslide Reactivation in March 2016 and Discussion of Concurrent Causes (Northern Apennines, Italy). *Landslides* **2018**, *15*, 1881–1887. [CrossRef]
58. Piacentini, D.; Troiani, F.; Daniele, G.; Pizziolo, M. Historical Geospatial Database for Landslide Analysis: The Catalogue of Landslide Occurrences in the Emilia-Romagna Region (CLOCkER). *Landslides* **2018**, *15*, 811–822. [CrossRef]

59. Ciccarese, G.; Mulas, M.; Alberoni, P.P.; Truffelli, G.; Corsini, A. Debris Flows Rainfall Thresholds in the Apennines of Emilia-Romagna (Italy) Derived by the Analysis of Recent Severe Rainstorms Events and Regional Meteorological Data. *Geomorphology* **2020**, *358*, 107097. [CrossRef]
60. Regione Emilia-Romagna. Available online: https://geoportale.regione.emilia-romagna.it/ (accessed on 11 March 2024).
61. Köppen, W. *Grundriß der Klimakunde*, 2nd ed.; Walter de Gruyter and Co.: Berlin, Germany; Leipzig, Germany, 1931.
62. Tomozeiu, R.; Busuioc, A.; Marletto, V.; Zinoni, F.; Cacciamani, C. Detection of Changes in the Summer Precipitation Time Series of the Region Emilia-Romagna, Italy. *Theor. Appl. Climatol.* **2000**, *67*, 193–200. [CrossRef]
63. Tomozeiu, R.; Lazzeri, M.; Cacciamani, C. Precipitation Fluctuations during theWinter Season from 1960 to 1995 over Emilia-Romagna, Italy. *Theor. Appl. Climatol.* **2002**, *72*, 221–229. [CrossRef]
64. Pavan, V.; Tomozeiu, R.; Cacciamani, C.; Di Lorenzo, M. Daily Precipitation Observations over Emilia-Romagna: Mean Values and Extremes. *Int. J. Climatol.* **2008**, *28*, 2065–2079. [CrossRef]
65. Jongman, B.; Hochrainer-Stigler, S.; Feyen, L.; Aerts, J.C.J.H.; Mechler, R.; Wouter Botzen, W.J.; Bouwer, L.M.; Pflug, G.; Rojas, R.; Ward, P.J. Increasing stress on disaster-risk finance due to large floods. *Nat. Clim. Change* **2014**, *4*, 264–268. [CrossRef]
66. Gelmini, R.; Pellegrini, M. Le frane del bacino del F. Panaro. *Atti Soc. Nat. Mat. di Modena* **1969**, *100*, 112–149.
67. Tosatti, G. Una frana in arenarie fratturate e in argille con inclusi litoidi: La frana di Gaiato nell'Appennino modenese. *Atti Della Società dei Naturalisti e Matematici di Modena* **1982**, *113*, 67–90.
68. Istituto Superiore per la Protezione e la Ricerca Ambientale (ISPRA). Available online: https://www.isprambiente.gov.it/ (accessed on 20 March 2024).
69. Geudtner, D.; Torres, R.; Snoeij, P.; Davidson, M.; Rommen, B. Sentinel-1 system capabilities and applications. In Proceedings of the Geoscience and Remote Sensing Symposium (IGARSS), Quebec, QC, Canada, 13–18 July 2014; pp. 1457–1460. [CrossRef]
70. Chen, C.W.; Zebker, H.A. Phase unwrapping for large SAR interferograms: Statistical segmentation and generalized network models. *IEEE Trans. Geosci. Remote* **2002**, *40*, 1709–1719. Available online: https://ieeexplore.ieee.org/document/1036000 (accessed on 17 July 2024). [CrossRef]
71. Crosetto, M.; Solari, L.; Balasis-Levinsen, J.; Casagli, N.; Frei, M.; Oyen, A.; Moldestad, D.A. Ground deformation monitoring at continental scale: The european ground motion service. *Int. Arch. Photogramm. Remote Sens. Spatial Inf. Sci.* **2020**, *XLIII-B3-2020*, 293–298. [CrossRef]
72. Crosetto, M.; Solari, L.; Mróz, M.; Balasis-Levinsen, J.; Casagli, N.; Frei, M.; Oyen, A.; Moldestad, D.A.; Bateson, L.; Guerrieri, L.; et al. The Evolution of Wide-Area DInSAR: From Regional and National Services to the European Ground Motion Service. *Remote Sens.* **2020**, *12*, 2043. [CrossRef]
73. Costantini, M.; Minati, F.; Trillo, F.; Ferretti, A.; Novali, F.; Passera, E.; Dehls, J.; Larsen, Y.; Marinkovic, P.; Eineder, M.; et al. European ground motion service (EGMS). In Proceedings of the 2021 IEEE International Geoscience and Remote Sensing Symposium IGARSS, Brussels, Belgium, 11–16 July 2021; IEEE: Piscataway, NJ, USA, 2021; pp. 3293–3296.
74. European Environment Agency. Available online: https://egms.land.copernicus.eu/ (accessed on 17 July 2024).
75. Covello, F.; Battazza, F.; Coletta, A.; Lopinto, E.; Fiorentino, C.; Pietranera, L.; Valentini, G.; Zoffoli, S. COSMO-SkyMed an existing opportunity for observing the Earth. *J. Geodyn.* **2010**, *49*, 171–180. [CrossRef]
76. Mari, S.; Valentini, G.; Serva, S.; Scopa, T.; Cardone, M.; Fasano, L.; De Luca, G.F. COSMO-SkyMed second generation system access portfolio. *IEEE Geosci. Remote Sens.* **2018**, *6*, 35–43. [CrossRef]
77. Agenzia Spaziale Italiana. Available online: https://www.asi.it/en/earth-science/cosmo-skymed/ (accessed on 21 March 2024).
78. Hooper, A.; Bekaert, D.; Spaans, K.; Arikan, M. Recent advances in SAR interferometry time series analysis for measuring crustal deformation. *Tectonophysics* **2012**, *514–517*, 1–13. [CrossRef]
79. Mancini, F.; Grassi, F.; Cenni, N. A workflow based on SNAP–StaMPS open-source tools and GNSS data for PSI-Based ground deformation using dual-orbit sentinel-1 data: Accuracy assessment with error propagation analysis. *Remote Sens.* **2021**, *13*, 753. [CrossRef]
80. Blewitt, G.; Hammond, W.C.; Kreemer, C. Harnessing the GPS data explosion for interdisciplinary science. *Eos* **2018**, *99*. [CrossRef]
81. Righini, G.; Pancioli, V.; Casagli, N. Updating landslide inventory maps using Persistent Scatterer Interferometry (PSI). *Int. J. Remote Sens.* **2012**, *33*, 2068–2096. [CrossRef]
82. Berti, M.; Corsini, A.; Pizziolo, M.; Tommaso, S.; Ciccarese, G.; Critelli, V.; Dal Seno, N.; Fabbiani, C.; Generali, M.; Ioriatti, E.; et al. Landslide inventory following the May 2023 Romagna hydrometeorological event (Northern Italian Apennines): The unavoidable requirement for laborious manual mapping. In Proceedings of the EGU General Assembly 2024, Vienna, Austria, 14–19 April 2024. EGU24-11385. [CrossRef]
83. Ministero dell'Ambiente e della Sicurezza Energetica. Available online: https://gn.mase.gov.it/portale/piano-straordinario-di-telerilevamento (accessed on 17 July 2024).
84. Dai, K.; Deng, J.; Xu, Q.; Li, Z.; Shi, X.; Hancock, C.; Wen, N.; Zhang, L.; Zhuo, G. Interpretation and sensitivity analysis of the InSAR line of sight displacements in landslide measurements. *GIScience Remote Sens.* **2022**, *59*, 1226–1242. [CrossRef]
85. van Natijne, A.L.; Bogaard, T.A.; van Leijen, F.J.; Hanssen, R.F.; Lindenbergh, R.C. World-wide InSAR sensitivity index for landslide deformation tracking. *Int. J. Appl. Earth Obs. Geoinf.* **2022**, *111*, 102829. [CrossRef]
86. Vecchi, E.; Tavasci, L.; Giorgini, E.; Gandolfi, S. A Priori Estimation of Radar Satellite Interferometry's Sensitivity for Landslide Monitoring in the Italian Emilia-Romagna Region. *Remote Sens.* **2024**, *16*, 2562. [CrossRef]

87. Farina, P.; Colombo, D.; Fumagalli, A.; Marks, F.; Moretti, S. Permanent Scatterers for landslide investigations: Outcomes from the ESA-SLAM project. *Eng. Geol.* **2006**, *88*, 200–217. [CrossRef]
88. Roa, Y.; Rosell, P.; Solarte, A.; Euillades, L.; Carballo, F.; García, S.; Euillades, P. First assessment of the interferometric capabilities of SAOCOM-1A: New results over the Domuyo Volcano, Neuquén Argentina. *J. S. Am. Earth Sci.* **2021**, *106*, 102882. [CrossRef]
89. Scipal, K.; Davidson, M. The SAOCOM-CS mission: ESA's first bistatic and tomographic L-band mission. In Proceedings of the 2017 IEEE International Geoscience and Remote Sensing Symposium (IGARSS), Fort Worth, TX, USA, 23–28 July 2017; IEEE: Piscataway, NJ, USA, 2017; pp. 123–124. [CrossRef]
90. Davidson, M.; Iannini, L.; Torres, R.; Geudtner, D. New Perspectives for Applications and Services Provided by Future Spaceborne SAR Missions at the European Space Agency. In Proceedings of the IGARSS 2022—2022 IEEE International Geoscience and Remote Sensing Symposium, Kuala Lumpur, Malaysia, 17–22 July 2022; pp. 4720–4723. [CrossRef]